Sea Ice - Atmosphere Interaction

Application of Multispectral Satellite Data in Polar Surface Energy Flux Estimates

K. Steffen, J. Key, J. Maslanik, M. Haefliger, C. Fowler
Cooperative Institute for Research in Environmental Sciences
Division of Cryospheric and Polar Processes
Campus Box 216, University of Colorado at Boulder

NAGW - 2158

Annual Progress Report
to
National Aeronautics and Space Administration

February 1992

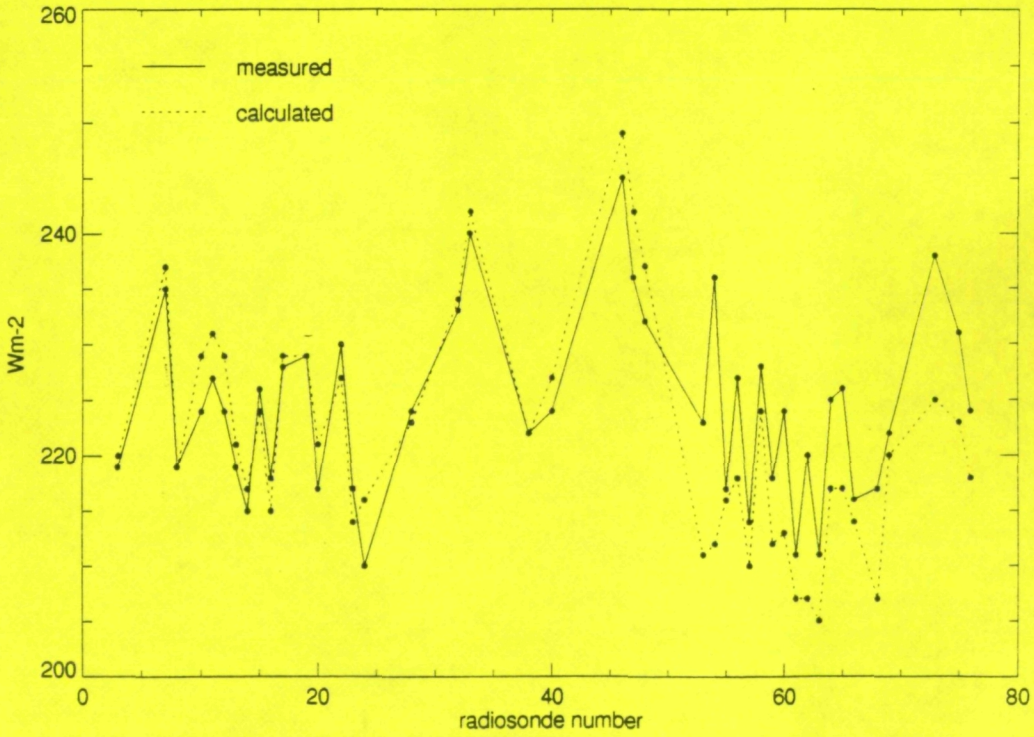

Calculated longwave radiation (LOWTRAN 7) with in situ radiosonde profile measurements compared to ground-based pyrano/pyrradiometer measurements.

TABLE OF CONTENT

APPENDIX:

Reprints of papers or draft papers

Emery, W.J., M. Radebaugh, C.W. Fowler, D. Cavalieri, and K. Steffen. An intercomparison of sea ice parameters computed from AVHRR and Landsat satellite imagery and from airborne passive microwave radiometry. *J. Geophys. Res.*, 96(C12), 22075-22086, 1991.

Maslanik, J.A., and J. Key, Fetch and stability sensitivity in large-area estimates of turbulent heat flux over sea ice, *submitted to J. Geophys. Res.*

Schweiger, A.J. and J. Key. Comparison of ISCCP-C2 and Nimbus-7 satellite-derived cloud products with a surface-based cloud climatology in the arctic. Accepted for publication *J. Climate*, February 1992.

Steffen, K., Energy flux density estimation over sea ice based on satellite passive microwave measurements, *Annals of Glaciology*, 15, 178-183, 1991.

Steffen, K. and A. Schweiger. NASA team algorithm for sea ice concentration retrieval from Defense Meteorological Satellite Program special sensor microwave imager: comparison with Landsat satellite data. *J. Geophys. Res.*, 96(C12), 21971-21987, 1991.

Steffen, K., and A. Schweiger. Application of passive microwave satellite data in arctic climate research. Glaciological Data, World Data Center A for Galciology, Univ. of Colorado at Boulder, (in press).

1. ICE SURFACE TEMPERATURE RETRIEVAL FROM AVHRR TIR

Jeff Key and Marcel Haefliger

Satellite data for the estimation of radiative and turbulent heat fluxes is becoming an increasingly important tool in large-scale studies of climate. One parameter needed in the estimation of these fluxes is surface temperature. Sea and land surface temperature (SST and LST) retrieval algorithms have been developed using the thermal infrared window portion of the spectrum, with the degree of success dependent primarily upon the variability of the surface and atmospheric characteristics. The general approach to estimating surface temperature is to relate satellite observations to surface temperature observations with a regression model. Lacking sufficient observations, however, satellite radiances or brightness temperatures can be modeled by application of the radiative transfer equation. This approach is commonly used for SST retrieval.

To our knowledge, little effort has been directed to the retrieval of the sea ice surface temperature (IST) in the Arctic, an area where the first effects of a changing climate are expected to be seen. The reason is not one of methodology, but rather our limited knowledge of atmospheric temperature, humidity, and aerosol profiles, the microphysical properties of polar clouds, and the spectral characteristics of the wide variety of surface types found there. We have developed a means to correct for the atmospheric attenuation of satellite-measured clear sky brightness temperatures used in the retrieval of ice surface temperature from the split-window thermal channels of the advanced very high resolution radiometer (AVHRR) sensors on-board three of the NOAA series satellites. These corrections are specified for three different "seasons" and as a function of satellite viewing angle, and are expected to be applicable to the perennial ice pack in the central Arctic Basin (Fig. 1.1). We do not develop a completely new methodology; instead we modify a standard procedure for use with Arctic-specific data. In this analysis it is assumed that a valid cloud-clearing algorithm exists and that only clear sky radiances are being examined. The cloud clearing problem in polar satellite data is not trivial, however. For a review of polar cloud detection algorithms, see *Key and Barry* [1989] and *Sakellariou et al.* [in press].

1.1 Data

Analyses are based on atmospheric temperature and humidity profiles collected by rawinsonde from a Soviet ice island (NP-26), located at approximately 85° N 170° W during 1983-1987 (Fig. 1.1). Generally two observations per day were collected covering a vertical range of 0-25 km. Profiles that have at least 10 levels are retained in the analysis. Observations include temperature, dew point depression, wind speed, and wind direction. For the years 1986-87 surface-based cloud observations are also available. These observations include low, middle, and high cloud types, height of the cloud base, and cloud fraction. Only clear sky profiles are of interest in this study, since the satellite thermal radiances under cloudy conditions will reflect cloud top temperature and a significant amount of cloud cover will affect the lower tropospheric temperature structure. Clear sky "seasons" that differ in their vertical temperature and humidity

structures are then defined. The seasons are determined objectively with a squared Euclidean distance clustering algorithm; the variables are temperature and humidity at each level. To reduce the degree of statistical dependence between levels, only one measurement per kilometer was used. The resulting seasons are winter: October through March, summer: June through August, and transition: April, May, and September. The resulting mean seasonal temperature profiles for clear, cloudy (greater than 75% cloud cover), and mixed conditions are shown in Figure 1.2.

1.2 Retrieval Methodology

For the retrieval of IST a multi-channel algorithm that uses empirical relationships to correct for water vapor absorption is employed:

$$T = a + bT_4 + cT_5 + d((T_4 - T_5) \sec \Theta)$$

where T_4 and T_5 are the satellite-measured brightness temperatures (K) in the AVHRR thermal channels and Θ is the sensor scan angle. The coefficients are determined through a least squares regression procedure, where surface temperatures are regressed against modeled brightness temperatures.

To simulate radiances in the AVHRR thermal channels, the daily temperature and humidity profiles in each season are used with the LOWTRAN 7 radiative transfer model [*Kneizys et al.*, 1988]. Radiances are modeled for sensor scan angles from 0° to 60° in 10° increments. The appropriate sensor response function is applied to the calculated radiances, and radiances are then converted to brightness temperatures. Atmospheric chemical composition, background tropospheric and stratospheric aerosols for the subarctic winter and summer models are used, since no such information is available from the ice islands. The optical properties of Arctic haze have not been extensively measured; model calculations [*Blanchet and List*, 1983] show that the volume extinction coefficient of Arctic haze is generally of the same order of magnitude as that of the tropospheric aerosols. Therefore, the use of tropospheric background aerosols is appropriate.

Directional surface emissivities for snow are modeled [*Dozier and Warren*, 1982]: the single scattering albedo and asymmetry factor in the scattering phase function are calculated from the Mie equations and the directional, wavelength-dependent emissivities are derived from the delta-Eddington approximation to the equation of radiative transfer. The directional emissivities are then integrated with the response function for channel *i*:

$$\varepsilon_i(\Theta) = \frac{\int_{\lambda_1}^{\lambda_2} \varepsilon(\lambda,\Theta)\Phi_i(\lambda)d\lambda}{\int_{\lambda_1}^{\lambda_2} \Phi_i(\lambda)d\lambda}$$

where $\varepsilon(\lambda,\Theta)$ is the emissivity in direction Θ at wavelength λ and Φ is the sensor response function which is Φ outside of $[\lambda_1,\lambda_2]$.

The use of the rawinsonde profiles in modeling the surface temperature requires an additional step since the first measurement in each profile is the shelter temperature, not the surface temperature. Therefore, the (unknown) surface temperature for each profile is assigned a series of values representing the range of possible surface temperatures for the observed conditions during the month to which the profile belongs. An energy balance model [*Maykut*, 1982] is used to determine these surface temperatures, based on the observed range of shelter temperatures and wind speeds (the mean +-1 standard deviation) in the ice island data for each month. The retrieval methodology is summarized in Figure 1.3.

1.3 Results

The seasonal dependence of the coefficients is illustrated in Table 1.1, where coefficients from each season were applied to data from every other season. Results are shown for NOAA 9 and indicate errors between 0.1° K for transition coefficients with winter data and 0.6° K when summer coefficients are used with winter data. Similarly, the satellite dependence of the coefficients is shown in Table 1.2 for summer conditions. On the average, errors ranging from 0.1 to 1.0° K, depending on season, can be expected when applying coefficients derived for one satellite to data from another, the smallest errors occurring between NOAA 7 and 9 coefficients and data. Using SST coefficients developed for the North Atlantic and the Greenland Sea area to estimate IST would result in an underestimate of up to 0.7° K, largest in winter and at scan angles of 40° and greater. While the sensor scan angle is included explicitly in the correction equation, its effect in the dry Arctic atmosphere is small, generally less than 0.1° K.

Surface temperature measurements taken by a PRT-5 thermal radiometer during CEAREX in March 1989 were compared to estimated ISTs from NOAA 11 AVHRR data. The mean IST for a sample of four AVHRR pixels was 258.9° K while the mean PRT-5 temperature (adjusted for an emissivity of 0.998) of four consecutive measurements one kilometer apart was 259.0° K. Given the difficulties in comparing the two data sets these results are encouraging.

1.4 Conclusions

Using the split window channels and scan angle, the rms error in the estimated ice surface temperature is less than 0.1° K in all seasons. Inclusion of channel 3 (3.7 μm) during the winter decreases the rms error by less than 0.003° K. Overall, employing the IST coefficients results in increased accuracy of up to 0.6° K over SST coefficients developed for the North Atlantic and the Greenland Sea areas.

TABLE 1.1 RMS error in applying coefficients (NOAA 9) developed for one season (left) to data from another (top).

Data from:	Winter	Summer	Transition
Coefficients:			
Winter	0	0.403	0.128
Summer	0.587	0	0.342
Transition	0.117	0.219	0

TABLE 1.2 RMS error applying coefficients (summer) developed for one satellite (left) to data from another (top).

Data from:	NOAA 7	NOAA 9	NOAA 11
Coefficients:			
NOAA 7	0	0.272	0.655
NOAA 9	0.296	0	1.017
NOAA 11	0.682	0.961	0

Fig. 1.1 Average minimum (solid) and maximum (dashed) sea ice extent in the Arctic Ocean. Also shown is the area covered by the NP-26 drifting ice island.

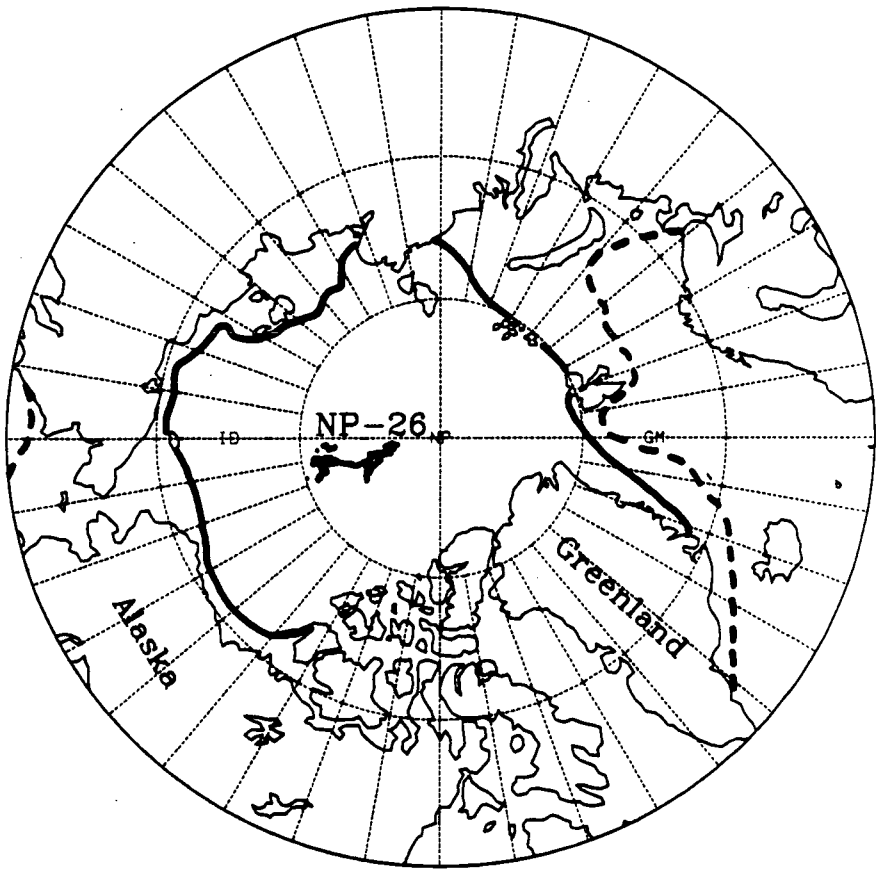

Fig. 1.2 Clear (solid), cloudy (dashed) and mixed (dotted) temperature profiles for the ice island data. (a) winter (October - March), (b) summer (June -August), and (c) transition (April, May, September).

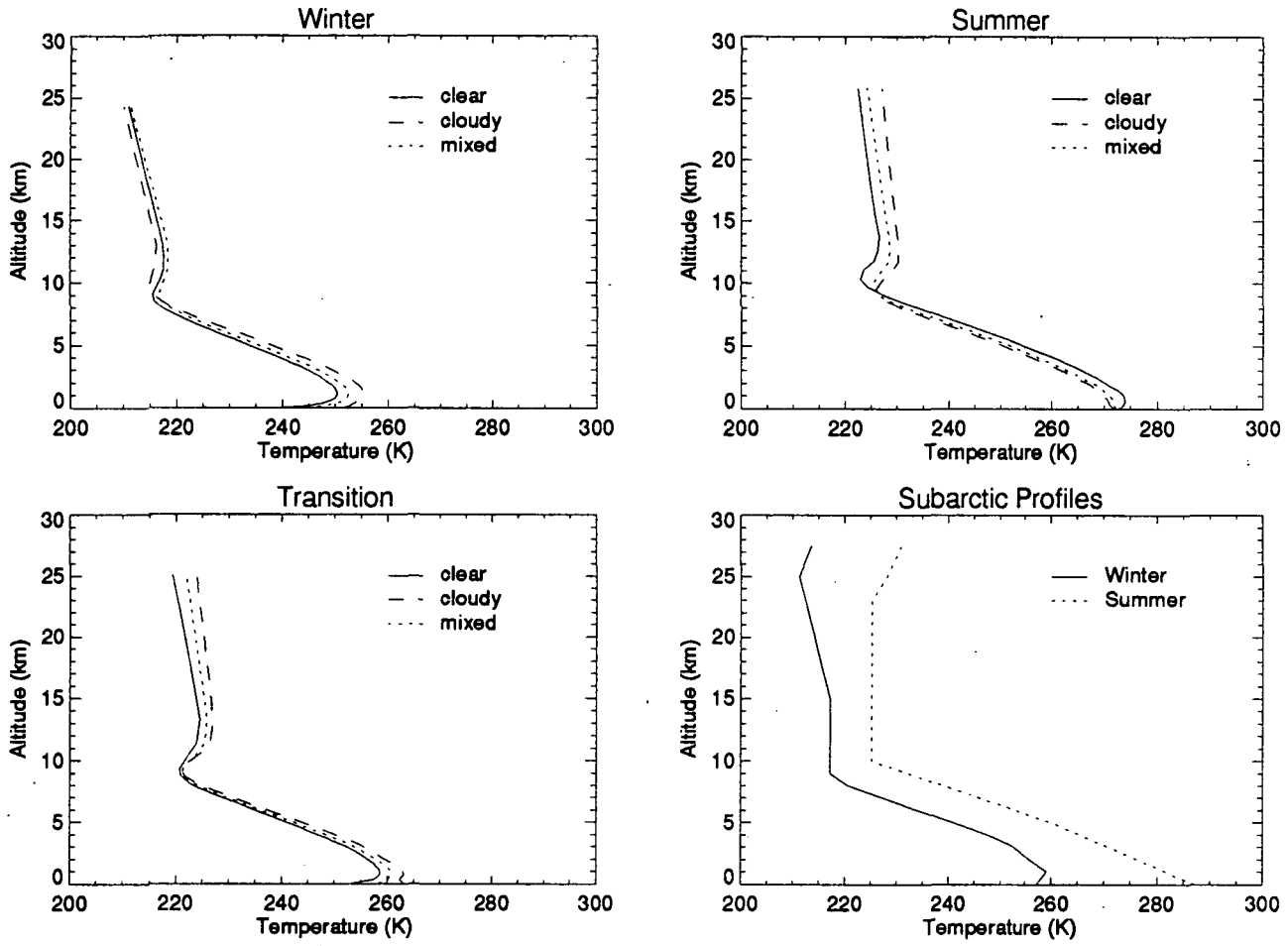

Fig. 1.3 Flow chart of the ice surface temperature retrieval methodology.

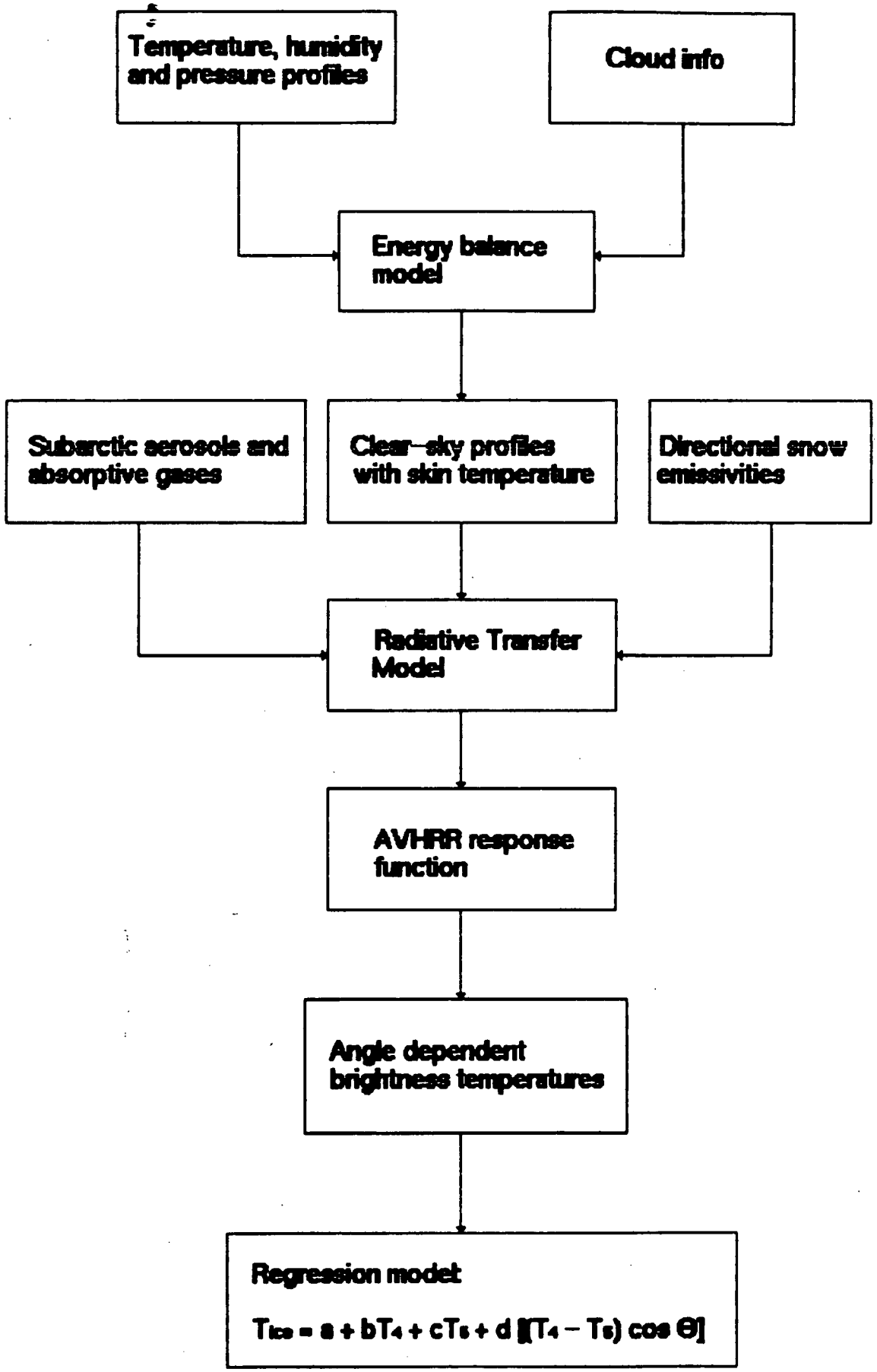

2. ICE SURFACE TEMPERATURES FROM PM-DATA

Jim Maslanik

The major problems with using passive microwave data to estimate IST are that 1) in most conditions, the microwave temperatures are from some ill-defined depth in the ice/snow column, and 2) emissivities at microwave frequencies are substantially more variable than at thermal frequencies. The advantages of passive microwave data are all-weather capability (or at least, much less sensitivity than thermal-wavelength data to atmospheric conditions) and reduced processing requirements. In addition, there is some value in knowing IST at different levels in the snow/ice column since, if surface and ocean fluxes and conductivities are known or can be estimated accurately, temperatures at different levels define the thicknesses of the ice and snow pack. Given these potential advantages and the fact that we are already developing a variety of data sets useful for evaluating IST, it appears worth some effort to examine passive microwave-derived IST.

2.1 IST Algorithm

The IST algorithm we use is an expansion of the approach described by *Cavalieri et al.* [1984], where:

$$T_{ice}(f) = ((T_B(f) - ((T_{water} * \varepsilon_{water}(f))*(1-C_{fy}-C_{my}))) / ((\varepsilon_{fy} * C_{fy})+(\varepsilon_{my} * C_{my})))$$

and f = frequency and polarization, ε = emissivity, C = concentration, T = physical temperature, T_B = brightness temperature, fy = first-year ice, and my=multiyear ice. By including the different ice types, we can estimate IST using all frequencies. The limitations of this simple method are that the emissivities and concentrations of the different ice types and open water must be provided. We use emissivities from the literature, and the NASA Team Algorithm to estimate ice concentrations. Our objective is to explore how well IST can be calculated given the uncertainty in these estimates. For the present, we are ignoring weather and atmospheric effects, as well as sensor miscalibrations. With this equation, errors in emissivity and concentration are straight multipliers contributing to the overall error. For example, a 10% error in ε_{fy} with C_{fy} = 0.4 and C_{my} = 0 yields an error in T_{ice} of about 4.6%. At C_{fy} = 0.9, the 10% e_{fy} error yields an 11% error in T_{ice}.

2.2 Data

The passive microwave data used for this experiment are an approximately eight-year record (Jan. 1979 - Nov. 1986) of SMMR data extracted from the CDMS optical-disk archive at NSIDC using the NODS software. The SMMR brightness temperatures were averaged over three-day intervals and 100 km x 100 km cell size, and converted to a format suited to our data visualization and analysis software. Data for comparison currently include temperatures from drifting buoys, drifting ice stations, gridded NMC temperatures, and the modeled IST described

in the previous section.

2.3 Passive Microwave-derived IST

As a first step, we calculated IST for the Arctic Basin for a single day (May 1, 1979), and focused on a transect of temperatures along the 150° meridian from the Alaska coast to about 84 ° N. T_{ice} at 6, 10, 18, and 37 GHz V pol. averaged along this transect was 265.9°, 265.5°, 264.2 °, and 260.2° K, respectively. A Soviet drifting station at about 75° N, 174° W reported a surface air temperature of 260° K, mean monthly NMC surface air temperatures along approximately the same transect were 258° K and 262° K for April and May, and an average of buoy temperatures in the area was 261° K. The SMMR temperatures show the increase in temperature expected with decreasing frequency (e.g., temperatures deeper within the ice pack). If we assume that the 18 GHz temperature is the temperature at approximately the snow-ice interface and the 37 GHz temperature represents the near-surface temperature, we can calculate an energy balance of conducted heat at the snow-ice interface. With a ice bottom temperature of 270° K and using standard conductivities for ice and snow, an ice thickness of 2 m and a snowdepth of 0.12 m, which are reasonable values, would balance the equation for the observed case. Given the potential errors in this simple approach, these results are tentative at best. However, it at least does not discourage further study.

To this end, we have calculated IST in the same manner for the Arctic Basin for a eight-year period (1979-1986). Figures 2.1-2 show the resulting mean January IST based on 37 GHz V for individual grid cells in the Canada Basin and Beaufort Sea. Figure 2.3 shows January means for the Canada Basin site estimated using 6 GHz V. In comparison, monthly averages of drifting buoy observations (from daily grids) in the Canada Basin are approximately 233°, 252°, 250°, 247°, 247°, and 255° K for Jan. 1980 - 1984. Average buoy temperatures in the Beaufort Sea area for January are 245°, 251°, 254°, 252°, 248°, and 248° K. In the Canada Basin, the mean difference (IST at 37 GHz - Buoy) is 6.5° K. The difference is 3.4° K excluding 1979, where the low buoy temperatures may be questionable, while in the Beaufort Sea, the mean difference for 1979-1984 is 1.0° K. The IST are typically higher than the buoy temperatures at the Canada Basin site, but alternate between being higher and lower at the Beaufort Sea site. We can also compare the Canada Basin IST to an 8-year average of drifting station temperatures and buoy temperatures in the north-western Canada Basin. The drifting-station 8-year means for January, February, and March surface air temperatures are 241°, 241°, and 242° K, the means of all the buoy temperatures within a 1000 km radius of the station for the same months are 247°, 247°, and 249° K. The 8-year IST (37 GHz) means for January-March are 252°, 252°, and 250° K. Based on this initial comparison, mean IST appear to be within about 5° K of buoy temperatures. Compared to the January mean IST estimated by the ice model (Fig. 3.2), both the buoy temperatures and the passive microwave IST are several degrees higher. However, even a several degree difference may not be unexpected, given the parameterizations and climatologies used for the model run.

Our plans are to carry out a more detailed comparison of the IST, buoy data, and model fields, and to compare passive microwave-derived IST with IST calculated from AVHRR data. The

AVHRR comparison will include AVHRR GAC imagery for January 1984, and AVHRR LAC data co-registered to SSM/I imagery. One problem with the AVHRR comparison will arise from the need to adjust the AVHRR IST to represent ice only, rather than an ice/open water mixture.

Fig. 2.1 Ice surface temperatures estimated using SMMR passive microwave data (37 GHz V) for a 100 km^2 cell in the Canada Basin. January means for 1979 - 1986.

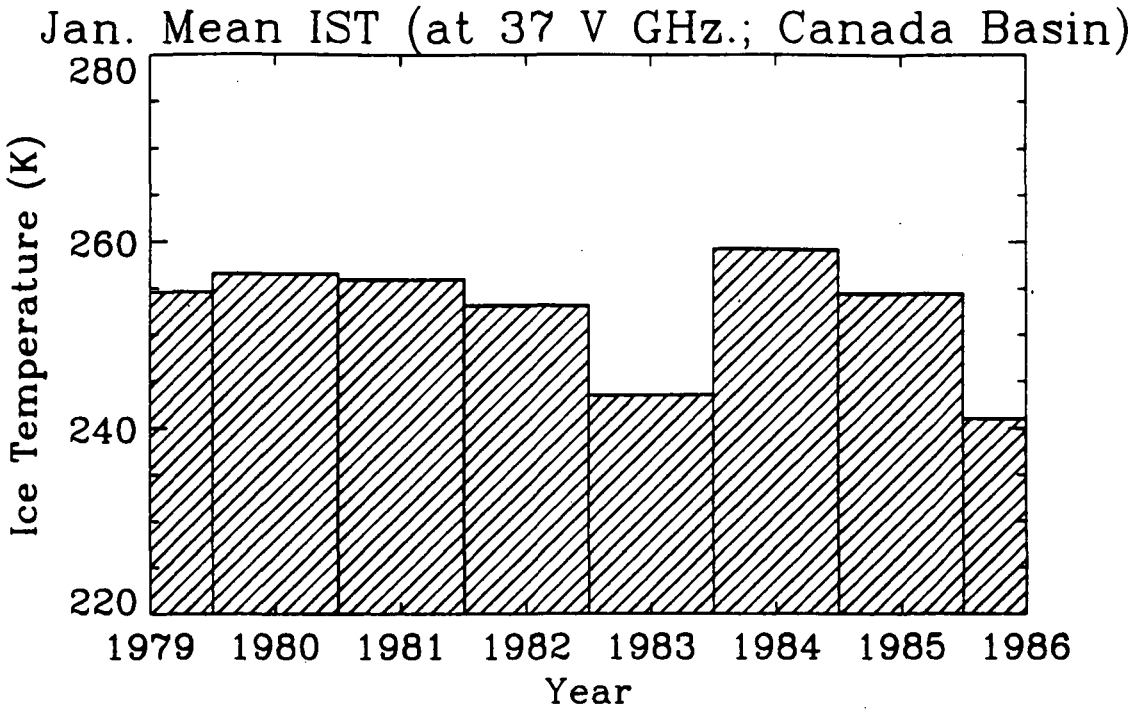

Fig. 2.2 Same as Figure 2.1, but for a cell in the Beaufort Sea.

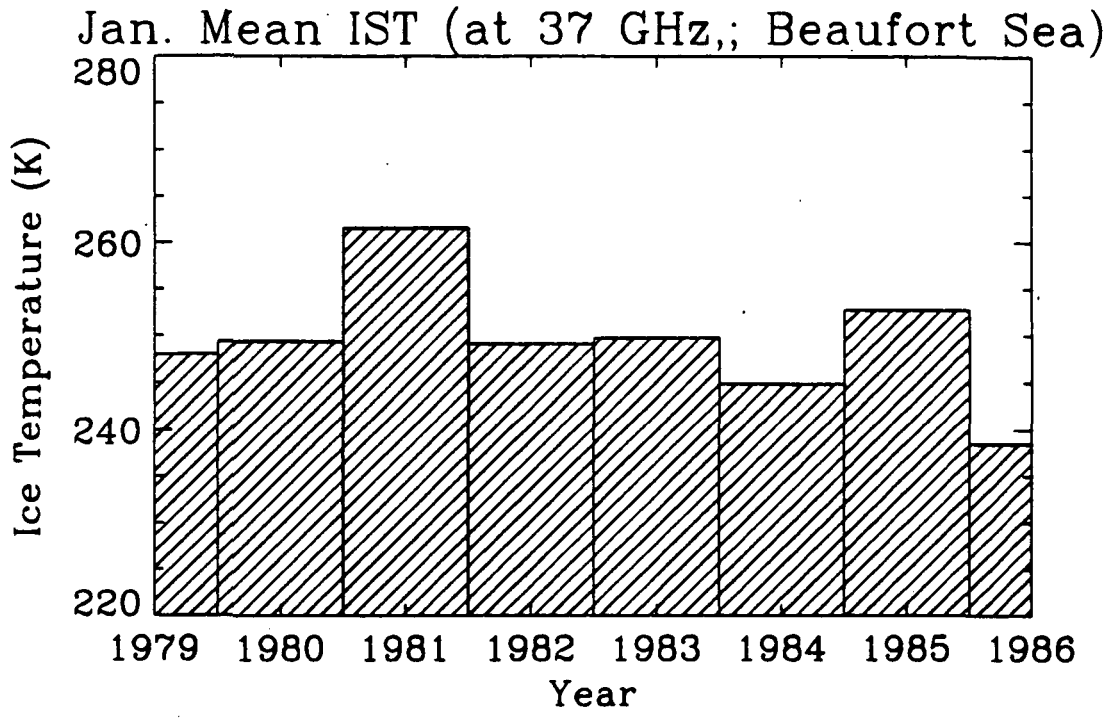

Fig. 2.3 Same as Figure 2.1, but using 6 GHz V. SMMR data for the Canada Basin cell.

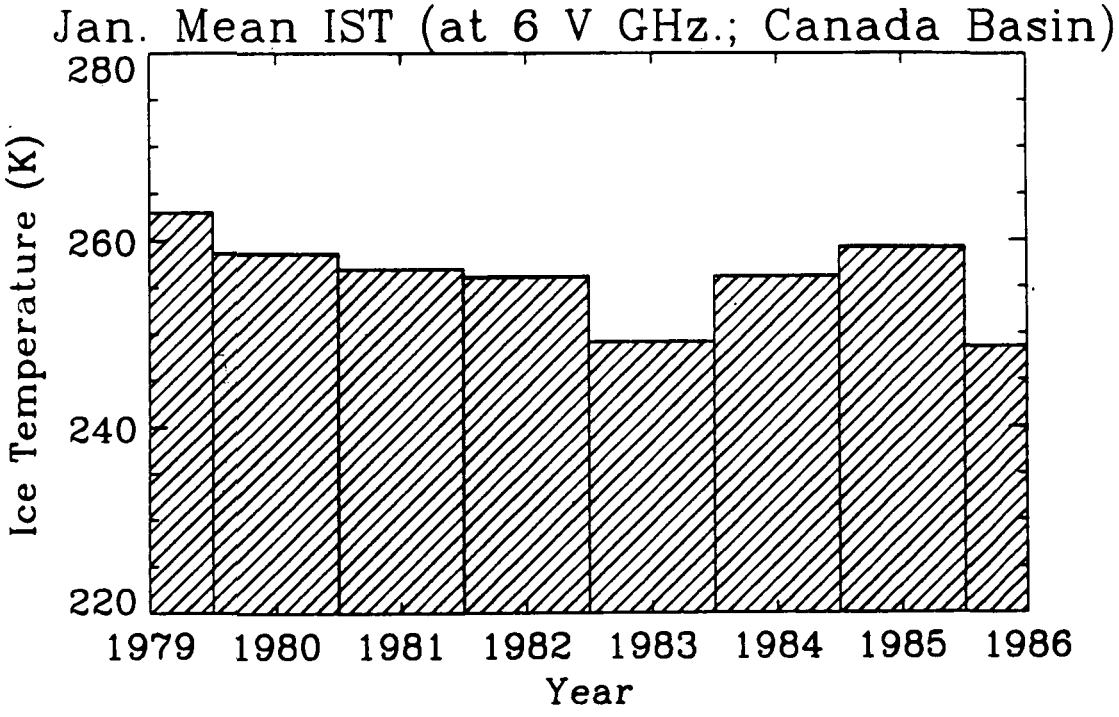

3. ICE MODELING INVESTIGATIONS

Jim Maslanik and Hilary Maybee

A valuable method of investigating the types of sensitivities required of remotely-sensed data for sea ice studies is to use a physical model of the ice cover to investigate how different sea-ice parameters vary under different conditions. In other words, the physical model should help define the natural variability of the sea ice system, and thus help determine the allowable error in satellite-derived data. This is an inversion problem, where an overall goal is to develop remotely-sensed data to improve modeling of the polar system, but in this case, we use an ice model to help us understand the remote sensing requirements. The parameters available to consider are ice surface temperature, ice concentration, ice type, and ice motion. Of these, we have begun by focusing on ice surface temperature, since ice surface temperature is the dominant variable controlling thermodynamic growth of the ice, whereas ice concentration and ice type are a result of a mixture of thermodynamic and dynamic processes, and thus subject to more modeling uncertainty. Ice motion is a function of ice dynamics alone, but ice motion is not a focus of our project.

Our objectives are:

- examine the day-to-day variability in modeled IST.
- examine the spatial variability of IST.
- generate IST fields that can be compared to remotely-sensed IST.

At this point, the model development allows us to consider the two first objectives.

3.1 Ice Model

The ice model used is a version of the cavitating fluid model developed by *Flato and Hibler* [1990], with a grid cell size of 160 km x 160 km. This 2-D dynamic-thermodynamic ice model is well-suited for climatological investigations and sensitivity studies since the cavitating-fluid ice rheology offers significant improvements in computation time compared to the viscous plastic rheology used in the original Hibler model [*Hibler*, 1979]. The thermodynamics of the model are nearly the same as that used by *Parkinson and Washington* [1979] with no explicit treatment of snow. In addition to this project, the ice model is being developed and used for a National Science Foundation project (in cooperation with Flato and Hibler at Dartmouth), and may be used for our NASA-funded ASF SAR investigations. Thus, there is some overlap in the modeling work, but each project benefits from the specific tests and model modifications made for each particular investigation.

In addition to minor code changes to install the model on our computers and to repair some run-time errors, we have modified the model to print out daily fields of calculated ice surface temperatures (IST), ice concentrations, and daily changes in ice concentration that exceed a specified threshold. Other modifications that are of value for this project are changes to separate ice concentrations and thicknesses into ice types using the methods of *Walsh and Zwally* [1990],

but revised to include second-year ice in addition to first-year and multiyear ice. We have also implemented an option to keep track of the source locations and ice type mixtures that flow into individual grid cells. Other modifications, including the use of the stability and fetch-adjusted transfer coefficients discussed in our earlier report, a coupling to the atmospheric boundary layer, explicit treatment of snow, more detailed radiative balance calculations, and an increase in model spatial resolution are either underway, planned, or being considered.

3.2 Forcing Fields

We are currently driving the model with daily geostrophic wind fields calculated from NMC data. Longwave fluxes, shortwave fluxes, and oceanic forcings are based on climatology and output from the Hibler-Bryan ice-ocean model [e.g., *Flato and Hibler*, 1990]. We would like to acknowledge the cooperation of Bill Hibler and Greg Flato who, in addition to providing us with the original model code, also gave us the ice-ocean model output and the climatological forcings. To date, we have prepared a 30-year record of daily wind forcings and monthly NMC 1000 mb temperatures. We also have drifting buoy fields and ECMWF gridded data available, but not yet reformatted to match the model grid. This also applies to the cloud cover data and calculated fluxes described elsewhere in this report.

3.3 Modeled Ice Surface Temperatures

Using daily winds for 1979, climatological radiative fluxes, constant oceanic flux, and daily time-stepping, IST is calculated as a function of modeled ice thickness. The model was cycled four times through the 1979 data to reach equilibrium. We present some preliminary results here. Figure 3.1 shows the resulting time series of daily ice surface temperatures for individual grid cells in the Beaufort Sea and the Central Arctic. Averages of day-to-day changes calculated for October, January, and April at the two locations are 0.3, 0.5, and 0.7° K (Beaufort Sea) and 0.4, 0.9, and 0.7° K (Central Arctic). The range and standard deviations of temperatures in January is 4.2° K and 0.9° K in the Central Arctic and 3.8° K and 0.8° K in the Beaufort Sea. It is somewhat surprising that the variability in IST in this example is greater within the central pack. Figure 3.2 shows the spatial distribution of mean January temperatures of ice. The change in IST per 100 km in this mean field is about 0.25° K / 100 km in the western Arctic and about 1.25° K / 100 km in the Fram Strait - East Greenland Sea.

The spatial and temporal variability of the modeled temperatures is of course controlled by the resolution of the model and of the forcing fields used in the thermodynamic calculations. Model results at this scale thus only provide a broad look at the distributions and magnitudes of IST. Even using these relatively low-resolution fields though, we can conclude that an IST algorithm for remotely-sensed data may need a precision of perhaps 0.2° K to capture most of the day-to-day variability in IST averaged over regions of about 160 km^2, while an absolute accuracy of about 1° K should be able to represent the large-scale temperature patterns. From these results, we can also get a rough idea of the range of IST that we should expect to see associated with reasonable ice thicknesses. Our plans are to further refine these estimates by driving the model with more accurate and detailed forcings.

Fig. 3.1 Annual time series of model-derived ice surface temperatures for grid cells in the central Arctic and Beaufort Sea.

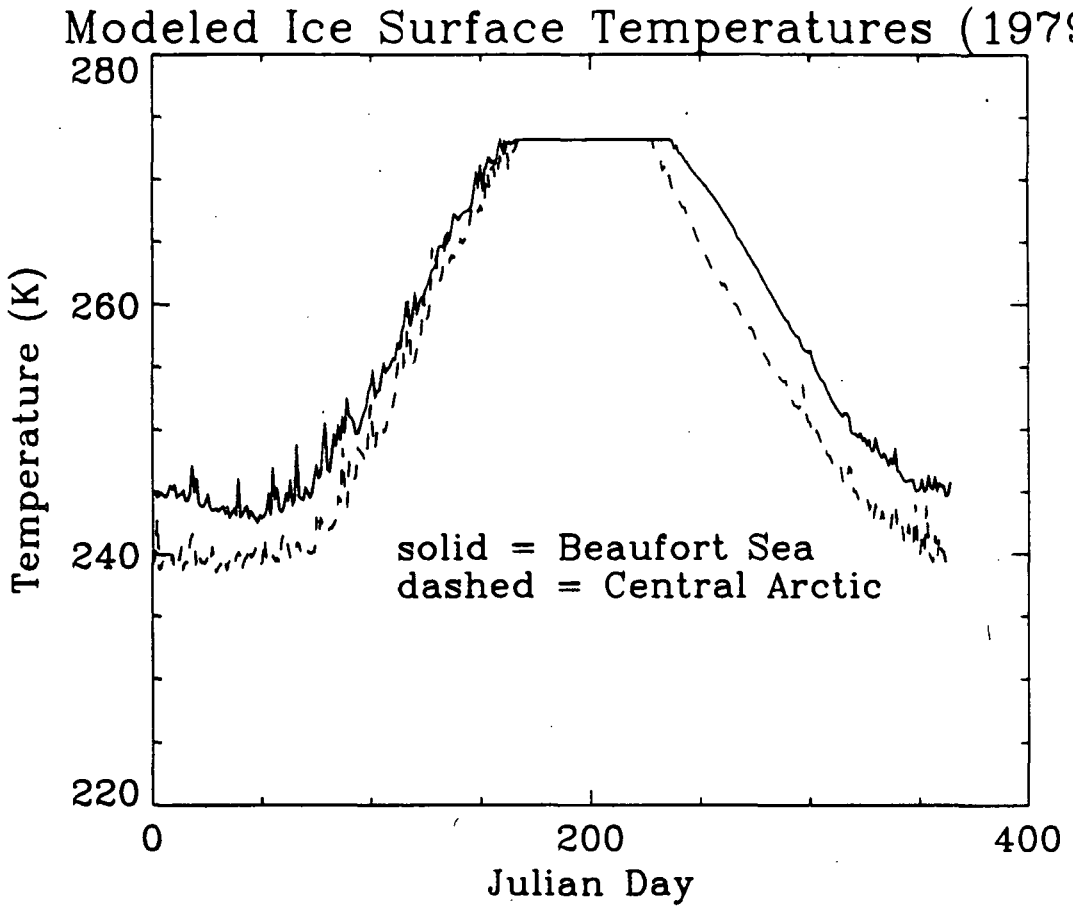

Fig. 3.2 Mean January ice surface temperatures estimated by the sea ice model using daily winds and climatological radiative fluxes.

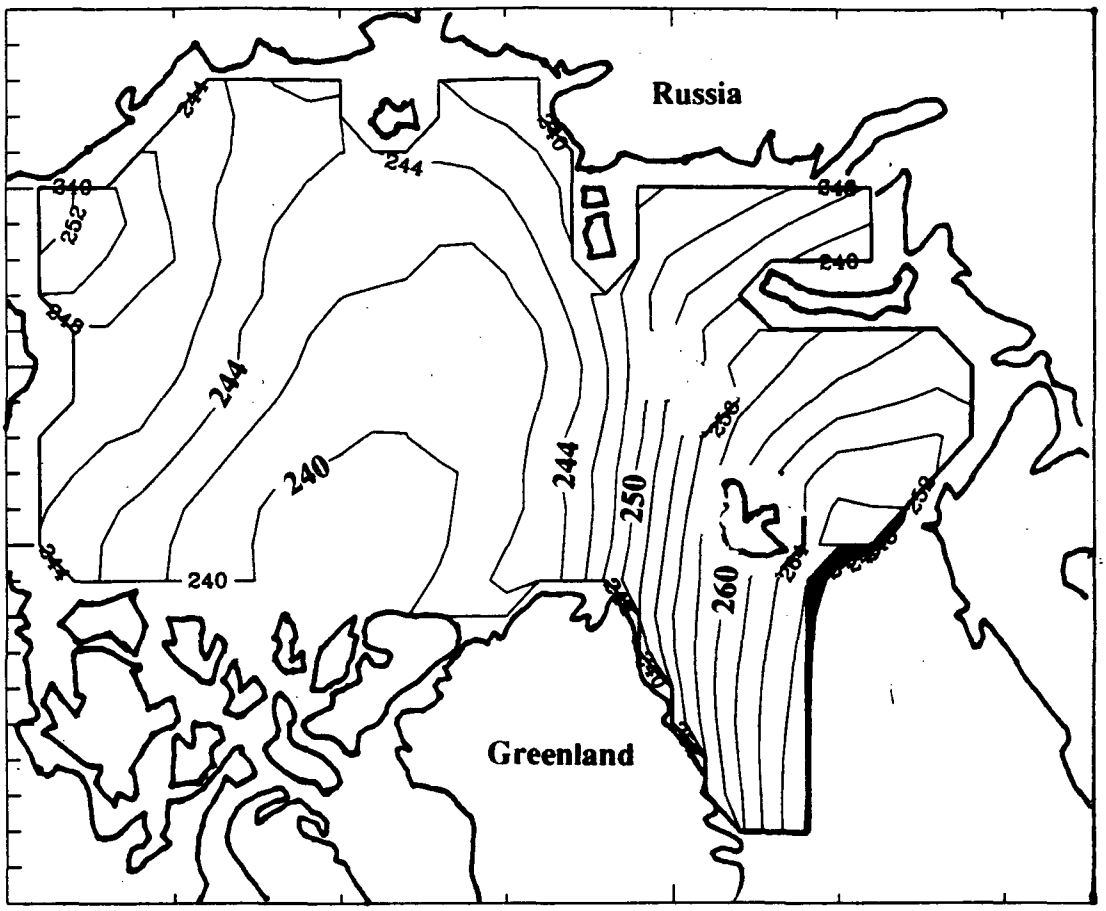

Contours = Ice surface temperature (K). Interval = 2K

4. VALIDATION OF LONGWAVE RADIATION MODELING

Marcel Haefliger and Konrad Steffen

The radiative transfer model LOWTRAN 7 calculates atmospheric transmittance, atmospheric background radiance, single scattered solar and lunar radiance, direct solar irradiance, and multiple scattered solar and thermal radiance. The spectral resolution of the model is 20 cm^{-1} in steps of 5 cm^{-1} from 0 to 50,000 cm^{-1}. LOWTRAN 7 uses a two stream approximation for multiple scattering and a k-distribution method to model molecular gaseous absorption. The multiple scattered thermal radiance option was used to calculate longwave irradiance for Greenland, based on a quadrature angle method as described by *Chandrasekhar* [1960]. To compute the irradiance the following formula was used:

$$I_{lw} = 2\Pi \sum_{i=1}^{i=n} a_i w_i$$

where a_i are the weights and w_i (lambda) the radiances calculated with LOWTRAN.

Table 4.1 shows the quadrature angles and weights applied to the LOWTRAN 7 model. The use of four different angles for the radiative transfer computation gives sufficient accuracy for this application. The single angle method at 52.5° as described by *Stearns et al.*, [1982] was also tested, but the results were not as good as with the four angles method.

Pressure, temperature and humidity were retrieved for a total of 43 radiosondes from the ETH camp. The vertical resolution of the profile was on the average 3 m, from 1300 to approximately 20,000 m. From this data set a standard profiles with 33 layers at 25 mbar intervals was generated. To account for absorption and emission due to CO_2, O_3 and aerosol, the standard subarctic summer profile was used. A sensitivity study showed that using standard subarctic winter or midlatitude summer profiles instead did not change the results significantly. The computation of the irradiance is more sensitive to small changes in the temperature and humidity along the profile. Comparison of modeled longwave radiation and ground measurements from the ETH camp showed a mean difference of 2.5 Wm^{-2} and a standard deviation of 6.3 Wm^{-2} for the 43 cases (Table 4.2 and Fig. 4.1). This analysis was carried out for clear days only.

Table 4.1 Angles and weights used to compute longwave irradiance with LOWTRAN 7.

Angle (a_i)	Weight (w_i)
81.966	0.031181
65.386	0.129847
43.684	0.203465
19.456	0.135507

Table 4.2 Measured and calculated longwave irradiances (Wm^{-2}) for clear sky condition from June to August 1990.

Radiosonde #	Date	Cloud Amount (octal)	Measured longwave Radiation (Wm^{-2})	Calculated longwave Radiation (Wm^{-2})
3	6-17	1	219	220
7	6-20	1	235	237
8	6-21	0	219	219
10	6-22	1	224	229
11	6-24	1	227	231
12	6-25	1	224	229
13	6-25	0	219	221
14	6-26	0	215	217
15	6-27	2	226	224
16	6-28	1	218	215
17	6-29	1	228	229
19	7-1	1	229	229
20	7-2	1	217	221
22	7-4	1	230	227
23	7-5	1	217	214
24	7-6	1	210	216
28	7-9	3	224	223
32	7-13	2	233	234
33	7-14	2	240	242
38	7-19	2	222	222
40	7-21	2	224	227
46	7-29	2	245	249
47	7-30	1	236	242
48	7-31	1	232	237
53	8-14	1	223	211
54	8-15	1	236	212
55	8-16	0	217	216
56	8-16	0	227	218
57	8-17	2	214	210
58	8-17	1	228	224
59	8-18	1	218	212
60	8-18	1	224	213
61	8-19	1	211	207
62	8-19	1	220	207
63	8-20	3	211	205
64	8-20	3	225	217
65	8-21	1	226	217
66	8-22	2	216	214
68	8-23	1	217	207
69	8-23	1	222	220
73	8-25	1	238	225
75	8-26	1	224	218
76	8-27	1	224	218

Fig. 4.1 Calculated longwave radiation based on LOWTRAN 7 radiative transfer model with in situ radiosonde profile measurements compared to ground-based pyrranometer longwave radiation measurements for the Greenland ice sheet at 1300 m a.s.l.

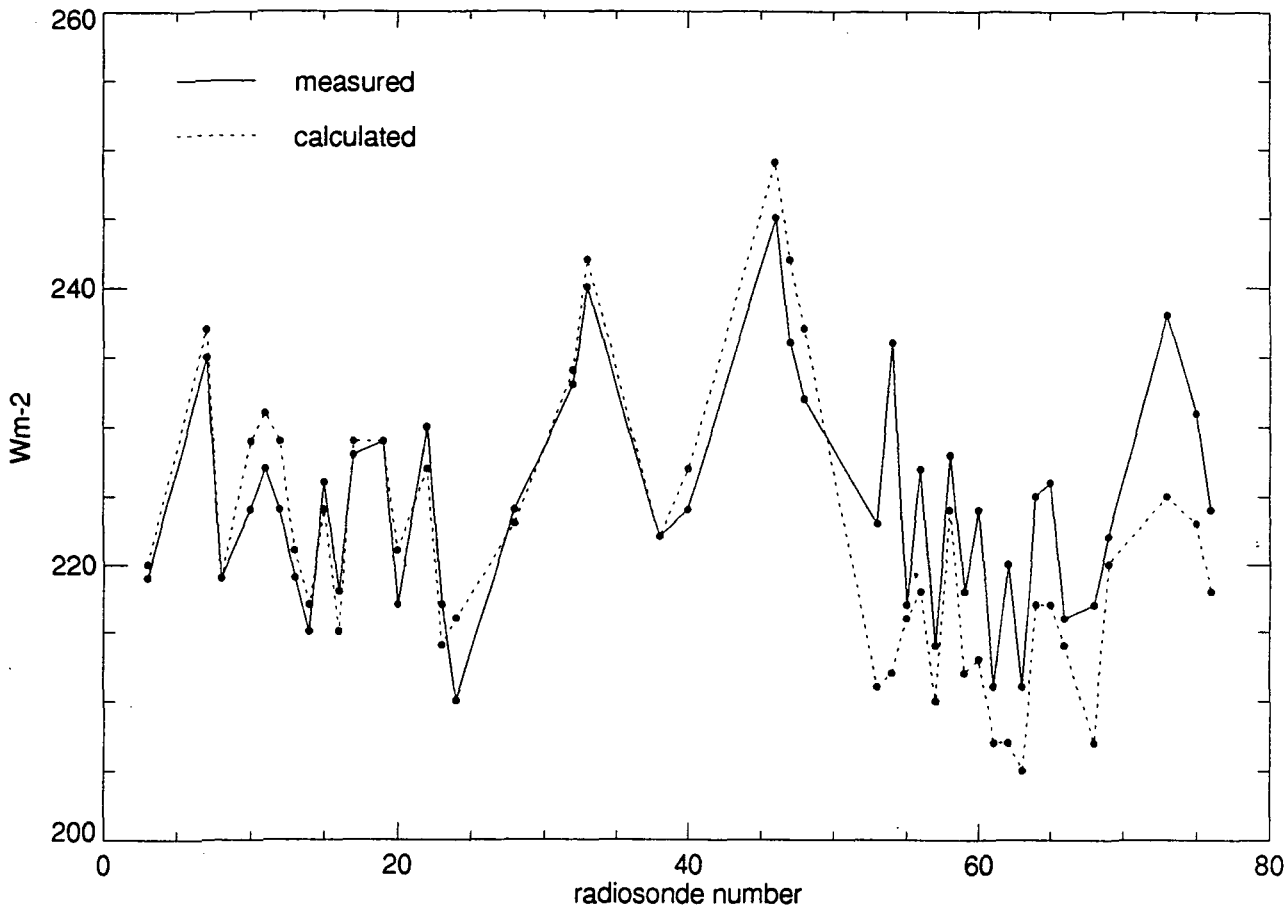

5. RADIATIVE FLUXES DERIVED FROM ISCCP-C2 DATA SET

Axel Schweiger

5.1 Objective and Approach

Information on radiative fluxes in the Arctic is sparse and originates mainly from a very limited number of observations from ice islands and a limited number of Arctic coastal stations. More detailed information with significant spatial coverage cannot be expected within the next 10-20 years. In order to quantify the Arctic radiation balance for large scale process studies such as sea ice modeling experiments as well as for comparison with GCM modeling studies, we have to rely on satellite remote sensing techniques which provide the only source of data with sufficient spatial and temporal coverage.

The main objective of this study is the compilation of a monthly climatology of Arctic radiative fluxes at the surface as well as at the top of the atmosphere. This climatology will represent a reevaluation of prior estimates and will incorporate the most recent data sets. The use of satellite-derived information will for the first time allow the investigation of the spatial variability of Arctic radiative fluxes. Radiative fluxes will be computed using a radiative transfer modeling approach, with the International Cloud Climatology (ISCCP) C2 data set as the main source of information on radiatively important atmospheric and surface properties.

Due to the limitations of satellite remote sensing techniques in retrieving radiatively important parameters, a secondary objective of this study focuses on determining the range of errors that we may expect due to deficiencies in the input data set. The overall objective of this research can be summarized as :

- Develop a model that integrates data sets, data processing steps and radiative transfer models for the purpose of calculating large scale radiative fluxes in the Arctic.
- Compile a monthly radiation climatology for the Arctic using the ISCCP-C2 data set as the main data source.
- Conduct sensitivity studies and comparisons with previous compilations of radiative fluxes to obtain an estimate of the potential errors
- Identify possible ways to improve the accuracy of calculated fluxes with respect to remote sensing techniques used, data processing and presentation, and radiative transfer modeling approaches.

The general approach selected here can be viewed as "top down" and is quite similar to that apparent in the development of general circulation models. Top down in this context means that in spite of the inaccuracies in the input data sets and the uncertainties in the underlying assumptions, a complete model that accomplishes the given task, i.e. computing large scale radiative fluxes for the Arctic is constructed. Upon completion of the model, sensitivity studies can be conducted to identify the most critical input parameters and the most urgently needed information. In constructing the model, we expect to learn much about how to integrate various

data sources and models, and which improvements in the data sets and models need to be made to accomplish the task more accurately and efficiently. Through this process we expect to provide important feedback to researchers concerned with developing remote sensing techniques and compiling input data sets, while at the same time we will provide a increasingly improving product with merits to a number of applications.

5.2 Data sets and validation

The validation of the ISCCP data set for the Arctic regions has been limited to a few case studies based on comparisons with more sophisticated cloud retrieval algorithms using a greater number of spectral channels [*Raschke et al.*, in press]. A more general comparison of ISCCP cloud products with cloud information that was otherwise available seemed warranted. We therefore chose to compare the ISCCP cloud statistics with those obtained from surface observations [*Warren et. al.*, 1986, 1988] and another satellite cloud product [*Stowe et al.*, 1988]. The details of this comparison are contained in a separate paper submitted for publication to Journal of Climate which is attached in the appendix. The most significant findings are summarized below.

- ISCCP Cloud amounts are generally lower than those reported by surface observers by 10 % during winter and up to 20- 30 % in the summer (Fig. 5.1)
- Spatial patterns of cloudiness between surface observations and ISCCP data are in rough agreement. Areas of increased cloudiness over the Barents Sea, Norwegian Sea area and fewer clouds over Greenland are represented in both data sets. Central Arctic cloud amounts from the ISCCP data set winter are substantially greater during winter.
- The annual cycle of cloud amounts in the ISCCP data set shows a remarkable resemblance to a study by *Curry and Ebert* [in press] where a climatology of ice crystal precipitation is combined with surface observations reported by *Huschke* [1969] with a minimum in total cloudiness in May. We speculate that ice crystal precipitation which is not reported by surface observers constitutes a significant part of the winter time "cloudiness" in the ISCCP data set.
- Overall comparison indicates that in the absence of truth, cloud amounts from the ISCCP data set represent a reasonable lower bound of the estimate.

5.2.1 Atmospheric profiles from Ice Islands

Serreze et al. [in press] have compiled a data set of atmospheric vapor and temperature profiles from North Polar Drifting stations. Mean monthly profiles and low level temperature inversion statistics from this data set were used along with the atmospheric profile information contained in the ISCCP data set to produce temperature, humidity and ozone profiles for the subsequent radiative analysis. Since the vertical resolution of the TOVS temperature and humidity profiles is too coarse to represent the radiatively important low level inversion. The inversion statistics from the ice island data set were used to add a climatological inversion to the ISCCP profiles. The following procedure was used to reconstruct a more realistic temperature profile from the ISCCP data set.

ISCCP temperatures for the given levels, surface, 500 mb and 15 mb were assumed to be correct. A climatological low level inversion based on the ice island statistics was then inserted into the profile. This four-level profile was then interpolated linearly to a profile consisting of ca. 10 levels. The exact number of levels is determined by the constraint that no layer can have a vertical temperature gradient of greater than 10° K. This constraint was added in order to satisfy the limitations of a linear approximation of the Planck function in the presence of clouds.

In the presence of clouds one additional level, given by cloud height and the cloud top temperature is used in the above described scheme. Figures 5.2 and 5.3 show a comparison of radiosonde and ISCCP reconstructed profiles during January and July 1986. The low level inversion seems to be reasonably represented but the ISCCP tropopause height during winter is greatly exaggerated. We are currently investigating the cause of this problem and will determine its effect on the radiative transfer calculations. We expect no significant error in surface radiative fluxes arising from this error in the profiles because of the very low amounts of moisture present at this height. The following experiment was conducted to test the importance of the presence of a surface inversion. Downwelling longwave fluxes were calculated using the profiles reconstructed with the above outlined procedure and with a profile linearly interpolated between the levels reported in the ISCCP data set. In the presence of a climatological inversion, downwelling longwave fluxes averaged over all Januarys were 11 Wm^{-2} greater than without climatological inversion.

While the ISCCP-C2 data set reports temperature and pressure at 3 levels (4 in the presence of clouds), information on water vapor and ozone abundance is only reported in integrated columnar quantities. Standard subarctic profiles [*McClatchey et al.*, 1973] were used to reconstruct water vapor and ozone profiles from the total columnar amounts by assuming a constant ratio of layer to column amounts.

Due to computational limitations, the input data set was subsetted to represent all ice covered areas north of 75°. In the future we plan to extend this areas to all northern hemisphere areas that areas that can be potentially covered by sea ice. The Greenland ice sheet will be included. Even though a more complete radiation climatology that provides fluxes over land areas would be more desirable, additional complications will arise from the fact that additional surface types will have to be added to appropriately model surface reflectivity over land. We will therefore assign this objective a lower priority.

5.3 Radiative Transfer Model

The radiative transfer model used to calculate radiative fluxes in this study is that developed by *Tsay and al.* [1988] who validated the general approach using measurements from the Arctic stratus experiment.

5.3.1 Gas absorption

Gas absorption for water vapor, O_3, CO_2 and oxygen is parameterized using an Exponential Sum Fitting Technique [*Wiscombe and Evans*, 1977] with 24 bands at varying intervals without

overlap for the shortwave region, and 9 bands at 200 cm^{-1} intervals including overlap of gases for the longwave region.

5.3.2 Clouds

Cloud single scattering properties are parameterized as:

$$\omega = a + bRe;\ g = c+dRe;\ \beta = (e + fRe)LWC,$$

where ω, g, and β are the single scattering albedo, the asymmetry factor and the volume extinction coefficient, Re the effective radius, LWC the liquid water concentration, and a,b,c,d,e,f are constants determined by linear fits to results from Mie calculations for each spectral band over a range of cloud types. Clouds are represented as Mie scattering layers of variable thickness. Cloud physical height and optical thickness are set to the values reported in the ISCCP data set. Cloud physical thickness is calculated from the above parameterization with effective radius Re set to 10 μm and a liquid water concentration of 0.2 gm^{-3}. These values were chosen to be consistent with the ISCCP retrieval algorithm. Results of a sensitivity study assuming an effective radius of 5 μm are shown in Figure 5.4 and indicate a low sensitivity to this parameter since optical depths are fixed. During winter, when due to the lack of visible light, no cloud optical thickness is reported in the ISCCP data set, cloud optical thicknesses are set to the mean summer values.

In addition to total cloud amount, the ISCCP-C2 data sets contains information on clouds in 7 categories, based on optical depth and height. Due to computational constraints only total cloud amount is currently used in the calculation of radiative fluxes. For each grid cell separate calculations are performed for cloud free and cloudy conditions. Results are linearly averaged with the fractional area of cloud and clear sky as weights. This linear averaging, neglecting the effect of reflections from cloud sides and leakage of radiation through cloud walls, seems legitimate in the Arctic regions, where stratiform clouds dominate and cloudiness is generally high. Since only total clouds are used, no assumption for cloud overlap has to be made. At a later stage, we plan to use cloud overlap statistics compiled by *Henderson* [1967] to conduct sensitivity studies in comparison with other overlap assumptions.

5.3.3 Surface reflectivity

Since the ISCCP data set only provides a single channel (0.6 μm) measurement of surface reflectivity, for the remaining spectral bands have to be inferred from this measurement under the assumption of a particular surface type. For the present experiment, the surface was assumed to be a mixture of maximally 3 surface types. Surface types are selected depending on season from a catalog consisting of fresh snow, old melting snow, melt ponds, bare ice, and open water. Reflectivities for 24 shortwave bands were computed for the two snow types assuming Mie scattering of ice grains and soot particles [*Warren and Wiscombe*, 1980, *Wiscombe and Warren*, 1980], spectral reflectivties of meltponds and bare ice were taken from *Grenfell and Maykut* [1977] and open water reflectivies from [*Swain and Davis*, 1978]. Currently only the spectra for the two snow types vary with solar zenith angle. Bare ice and meltpond spectra are represented only for diffuse radiation. The fractional area covered by each surface type is determined in the

following way. Depending on month, maximally 3 surface types are selected. For example in June melting snow, meltponds and open water are the prescribed surface types. Given the channel 1 reflectivity, ice concentration contained in the ISCCP data set and precomputed reflectivties for the assumed surface types corresponding to the channel 1 wavelength interval, fractional area of meltponds can be calculated. If meltpond coverage assumes an unrealistic value of greater than 50% or during times where only snow and open water are the assumed to be the only present surface types, channel 1 snow reflectivities are adjusted to match observed values. Snow reflectivities in the remaining 23 Bands are adjusted under the assumption of constant ratios to channel 1 reflectivities. The fractional coverage of each surface type is then used to calculate the total surface reflectivity for all 24 bands.

5.4 Results

5.4.1 Downwelling short wave radiation at the surface

Figure 5.5 shows downwelling shortwave fluxes at the surface $R_s\downarrow$ from the ISCCP data set and those reported in a climatology by *Marshunova* [1961] as reported by *Fletcher* [1961], which was assembled from radiation measurements from measurements on Russian north polar drifting stations. The comparison indicates a remarkably close agreement between our calculations and Marshunovas measurements. In the first half of the year differences due not exceed 20 Wm^{-2} with the maximum difference in March. The greatest difference can be observed in July when $R_s\downarrow$ calculated from the ISCCP data set exceeds Marshunovas value by as much 50 Wm^{-2}. For the remainder of the year ISCCP fluxes are larger by no more that 30 Wm^{-2} which is consistent with the expected underestimation of cloud cover in the ISCCP data set. Figure 5.6 shows downwelling longwave fluxes at the surface $L_s\downarrow$ calculated from the ISCCP data set and those reported by Marshunova. A note has to be made with respect to her longwave "measurements". In her climatology of long wave fluxes in addition to measurements, Marshunova also uses downwelling longwave fluxes parameterized based on air temperatures and cloud information. This parameterizations were apparently developed from actual ice island measurements [*Curry and Ebert*, in press]. During winter when $L_S\downarrow$ is the only radiative input from the atmosphere to the surface. Differences between ISCCP and Marshunova fluxes are quite reasonable, with ISCCP fluxes exceeding those by Marshunova by no more than 20 Wm^{-2}. During spring when the atmospheric temperatures and cloudiness increase, differences between ISCCP calculated long wave fluxes and Marshunovas values also increase with the maxima of the differences in May and July. During this time our values of $L_S\downarrow$ are up to 60 W^{-2} lower than those reported by Marshunova. Again, this is consistent with the fact that ISCCP cloud amounts during summer would most likely be less than those used in Marshunovas calculations. Even though there is no exact correspondence and exact traceback to the original observations is difficult, cloud observations from Russian ice islands can be assumed to represent a significant part of the cloud statistics for the central Arctic contained in the Warren et. al. data set.

Figure 5.7 shows a comparison of the spatial pattern of $R_S\downarrow$ computed from the ISCCP data set with $Rs\downarrow$ for July from a climatology compiled by *Vohwinkel and Orvig* [1962]. The Vohwinkel and Orvig climatology covers a greater area that the area currently analyzed from the ISCCP data set. Generally ISCCP calculated values of are ca. 25-30 Wm^{-2} higher. Greater

values of $R_S\downarrow$ over the Greenland ice sheet are apparent in both data sets and is due to fewer clouds over this area. A minimum in $R_S\downarrow$ in the Barents-Norwegian sea area is apparent in both data sets. Differences in this area are smaller and in the order of 10 Wm^{-2} is probably to the fact that ice concentrations in this area are commonly lower which enhances the ability of the ISCCP algorithm to detect clouds. This hypothesis is supported by our finding that ISCCP cloud amount in this area also match surface observations more closely. The most striking feature in the comparison between ISCCP derived values of $R_S\downarrow$ and the Vohwinkel and Orvig climatology is the level of spatial detail. Two main spatial features aside from the ones mentioned above, can be noted in the ISCCP map. The area just north of Greenland that receives up to 345 Wm^{-2} and an area in the Laptev sea that receives only 270 Wm^{-2} of shortwave radiation compared with 300-320 Wm^{-2} downwelling in most of the central Arctic. It has to be noted that only 4 years of data are contained in the ISCCP data set and the spatial features described would not persist over longer time periods. Nevertheless it would be interesting to determine the effect of these spatial features on the sea ice regime. A sea ice modeling experiment will be conducted later to investigate this question.

5.4.2 Surface Albedo

Figure 5.8 shows the annual cycle of albedo from Marshunova along with the spectrally integrated albedo computed from the ISCCP data set. Prior to a comparison it should be noted that early spring and late fall values in the ISCCP data set should be neglected. They originate from inaccurately retrieved channel 1 reflectivities for poorly illuminated pixels located far north. The ISCCP algorithm currently does not retrieve surface reflectivities at solar zenith angles greater than 75°. Considering the above evidence, this cutoff should probably occur at a somewhat smaller zenith angle. In the future we will incorporate a mechanism into our processing stream that will eliminate erroneously low channel 1 visibilities over ice covered regions. The comparison of albedo values from surface observations and ISCCP indicates that albedoes measured directly on the ice are by up to 0.2 greater than those computed from the satellite derived visible reflectances. In fact, as shown in Figure 5.8, ISCCP channel 1 reflectances are even lower than spectrally integrated albedoes measured at the surface. There are several reasons for these difference. While to my knowledge being the only data set of albedo measurements for the entire annual cycle, Marshunovas sea ice albedoes seem high compared with the measurements of other researchers [*Grenfell and Maykut*, 1977]. This fact points to possible biases in the calibration or selection of measurement sites. Furthermore, ISCCP channel 1 reflectances represent integrated reflectances which contain a probable low bias due to the fact that the algorithm identifies surface pixels by their presumed lower reflectance. Open and refrozen, leads, meltponds, and bare ice contribute significantly to the integrated albedo. This difference between areally integrated albedoes and point measurement provides a possible explanation for the fact that albedoes from surface measurements increase past July, while those calculated from the ISCCP data set continue to decrease. In addition to the above mentioned problems another problem possibly related to our radiation transfer scheme becomes apparent when channel 1 reflectances are compared with the computed integrated albedoes. This difference related to the very low near infrared reflectivity of snow, seems too large when compared to the measurements and theoretical calculations of other authors [*Grenfell and Maykut*, 1977; *Wiscombe and Warren*, 1980]. While our computed differences between 0.6 μm reflectance and spectrally integrated albedo are in the range of 0.12 other authors report

differences in the order of less than 0.07. We are currently investigating the source of this discrepancy.

A comparison of our calculated albedoes with those parameterized from manually classified Defense Meteorological Satellite Program (DMSP) images [*Robinson et al.*, in press] shows an encouraging agreement in the spatial patterns (Fig. 5.9 and 5.10). Albedoes calculated from the ISCCP data set in May again are lower than those parameterized by Robinson et al., but the agreement in the spatial patterns with concentric contour lines and the area of higher albedo protruding towards the Bering Strait is remarkable. The quantitative disagreement between Robinson et al. and our calculations may in part be explained by the fact that their manual analysis only distinguishes 4 visually interpreted classes. An albedo of 0.8 is assigned to the most reflective class. In July again the similarity of the spatial pattern is striking but ISCCP albedoes are now higher than those by Robinson et al.

Since the capabilities of an interpreter in detecting over sea ice are expected to be superior to that of an automatic algorithm, we the previous result indicates that the ISCCP algorithm must perform quite well in identifying surface pixels.

5.4.3 Top of the atmosphere fluxes

Figure 5.11. shows calculated top of the atmosphere fluxes in the short and longwave regions. The radiation balance of the Arctic at the top of the atmosphere is negative throughout the year. During summer longwave losses are offset by shortwave gains so that total loss during June is no more that 20 Wm^{-2}. In winter, longwave losses of 180 Wm^{-2} account for a negative top of the atmosphere balance. Comparisons with measurements from the ERB experiment and other top of the atmosphere radiation climatologies will be presented at a later stage along with calculated cloud forcings.

5.5. Conclusions

Our investigations have so far produced several interesting results. Which are summarized below.

- Despite potential problems due to the difficulties in identifying clouds in the polar regions, the ISCCP data set seems to provide useful information on the temporal and spatial variability of radiatively important parameters. With respect to cloud amount, the ISCCP data set provides a reasonable lower bound of the estimate.
- Downwelling shortwave fluxes are in remarkable agreement with a climatology compiled from measurements.
- Differences in downwelling longwave radiation between our calculations and those of Marshunova are consistent with cloud.
- Spatial patterns of calculated surface albedoes agree well with a parameterization using visual interpretation manual classification. This is encouraging in so far as we may conclude from this that the ISCCP algorithm correctly distinguishes ice covered surfaces from clouds.
- The presence of a climatological inversions increases downwelling longwave fluxes by an

average of 11 Wm^{-2} over all four Januarys.

5.6 Further Plans

- Expand study area to include all potentially ice covered areas.
- Incorporate passive microwave derived ice concentrations to better represent surface reflectivity. Since the ISCCP data set reports ice concentrations derived from the Joint Ice Center ice charts, ice concentrations in the central Arctic are almost exclusively 100%. Even though passive microwave ice concentrations during the summer are most likely too low, their application to this problem will be investigated.
- In order to quantify the range of errors we may expect from inaccuracies in the input data set and the uncertainty of some of the underlying assumptions we will conduct a range of sensitivity studies. Currently planned sensitivity studies will address the most significant problem of the potential underestimation of cloud cover from the ISCCP data set. We will use the Warren et al. cloud data set to compute radiative fluxes, using optical depths, atmospheric profiles and surface parameters from the ISCCP data set. This calculations should at the same time provide another useful estimate that may be used in sea ice modeling experiments and indicate the sensitivity of our calculations to cloud amount. Another set of sensitivity studies will address the issue of parameterization of cloud overlap. Cloud overlap statistics from Henderson will be used.
- The sensitivity of flux calculations due to inaccuracies in the profiles and lack of vertical resolution will be tested further.
- One particular problem arises from the fact that ISCCP-C2 data represent monthly averages computed from 3 hourly data. Quantities area linearly averaged except for optical depth which is weighted according to an energy weighted scheme. We will investigate the effect of the decreased temporal resolution by using 2 month of C1 data one for winter one for summer for which we compute radiative fluxes on a daily bases before we averaging.
- More detailed comparisons with other data sets.
- Conduct sea ice modeling experiment to investigate the impact of errors in radiative fluxes on an application.

Fig. 5.1 Total Cloud Amount from the ISCCP-C2 (dashed - squares) and the *Warren et al.*, [1980] (solid-star) data sets. Marginal cloud amounts reported in the ISCCP-C2 data set is also displayed (dashed-circles). Note : This figure differs from figure 1. in the attached paper due to a processing error in the publication figure.

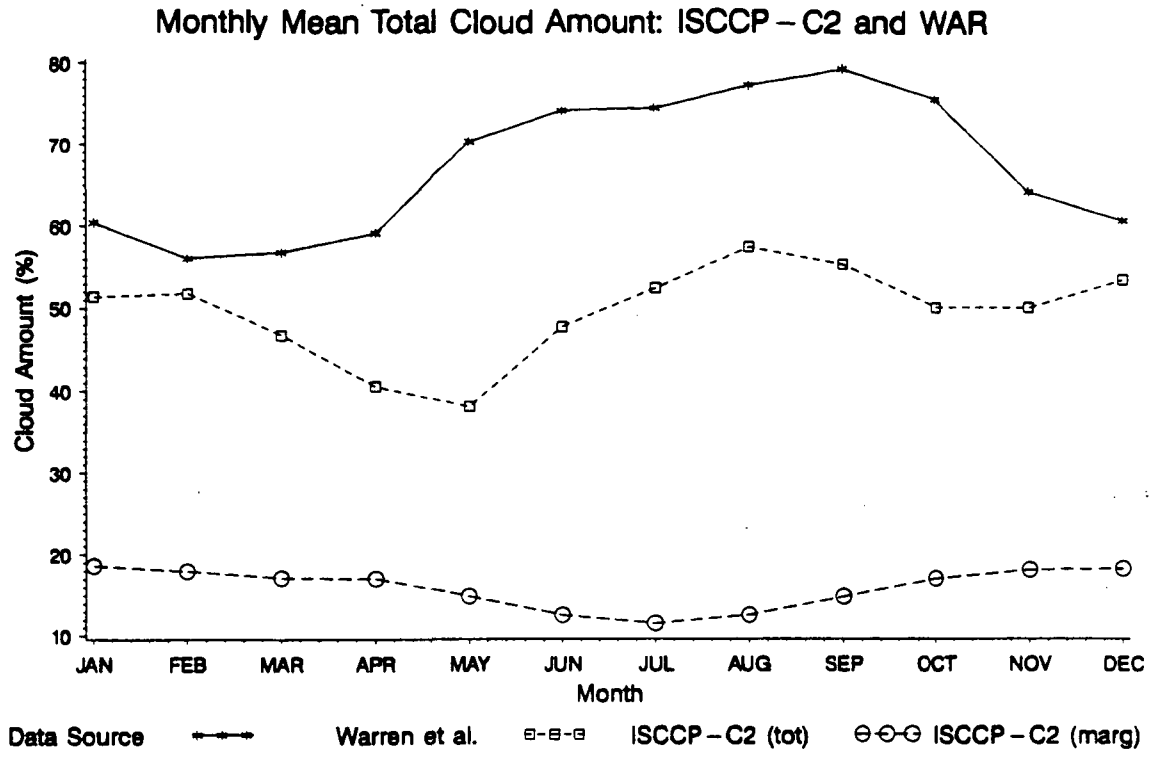

Fig. 5.2 Comparison of temperature profiles from north polar station NP-26 (solid) and ISCCP reconstructed profiles (dashed) in January 1986.

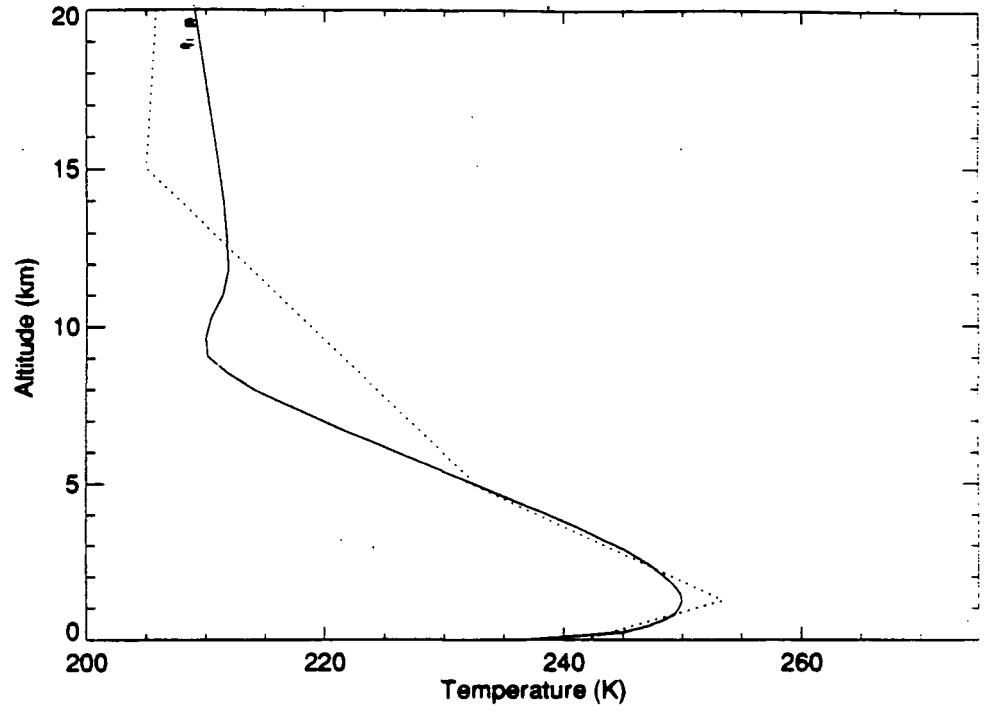

Fig. 5.3 Comparison of temperature profiles from north polar station NP-26 (solid) and ISCCP reconstructed profiles (dashed) in July 1986.

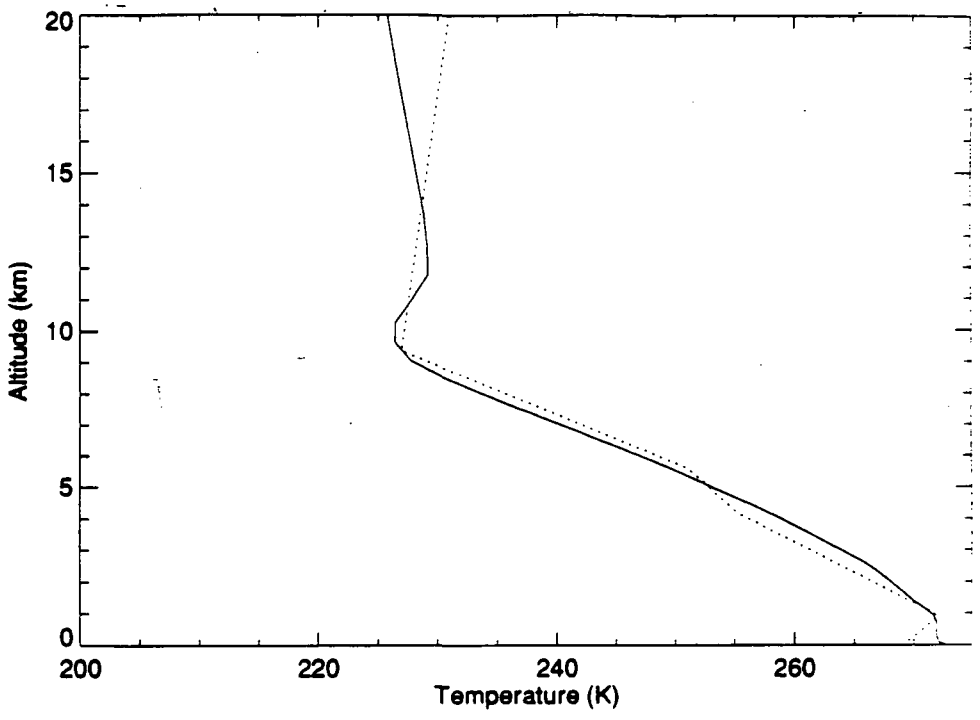

Fig. 5.4 Downwelling shortwave and longwave flux-densities at the surface computed from the ISCCP data set using a cloud droplet radius of 10 and 5 μm.

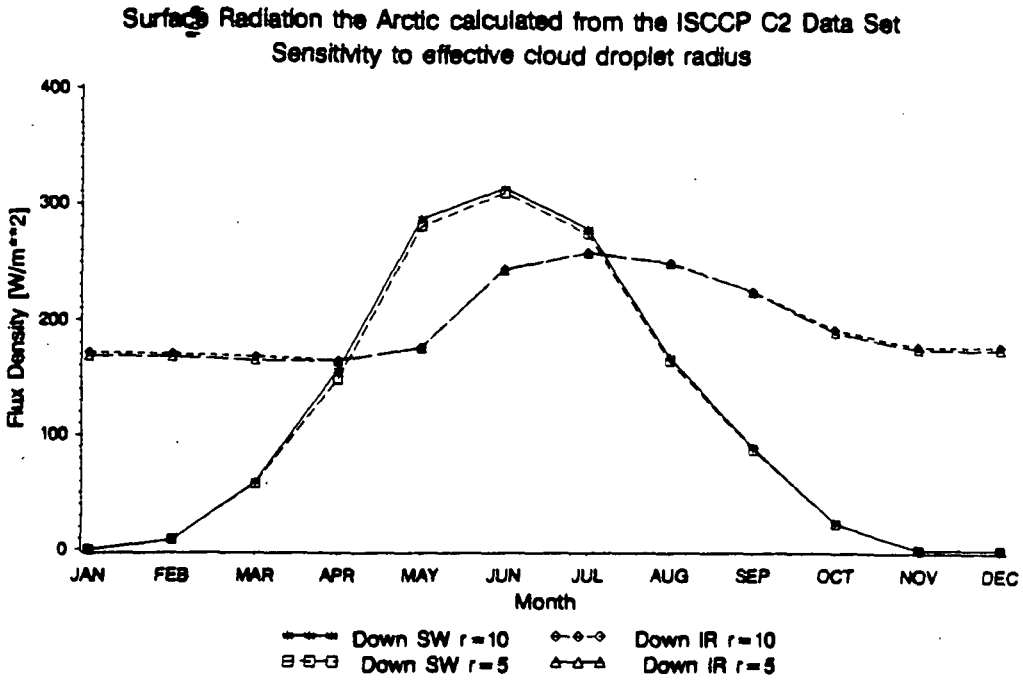

Fig. 5.5 Downwelling shortwave flux densities Rs↓ at the surface calculated from the ISCCP data set (dashed) compared with a climatology compiled from measurements on ice drifting stations by *Marshunova* [1961] (solid).

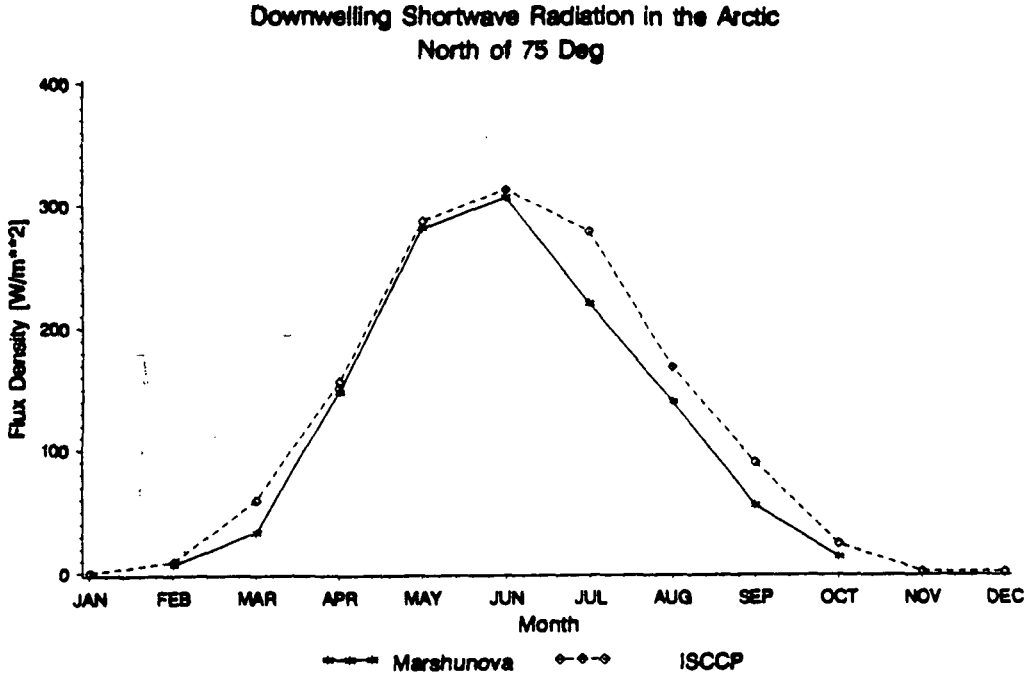

Fig. 5.6 Downwelling longwave flux densities $L\downarrow$ at the surface calculated from the ISCCP data set compared with a climatology compiled by *Marshunova* [1961].

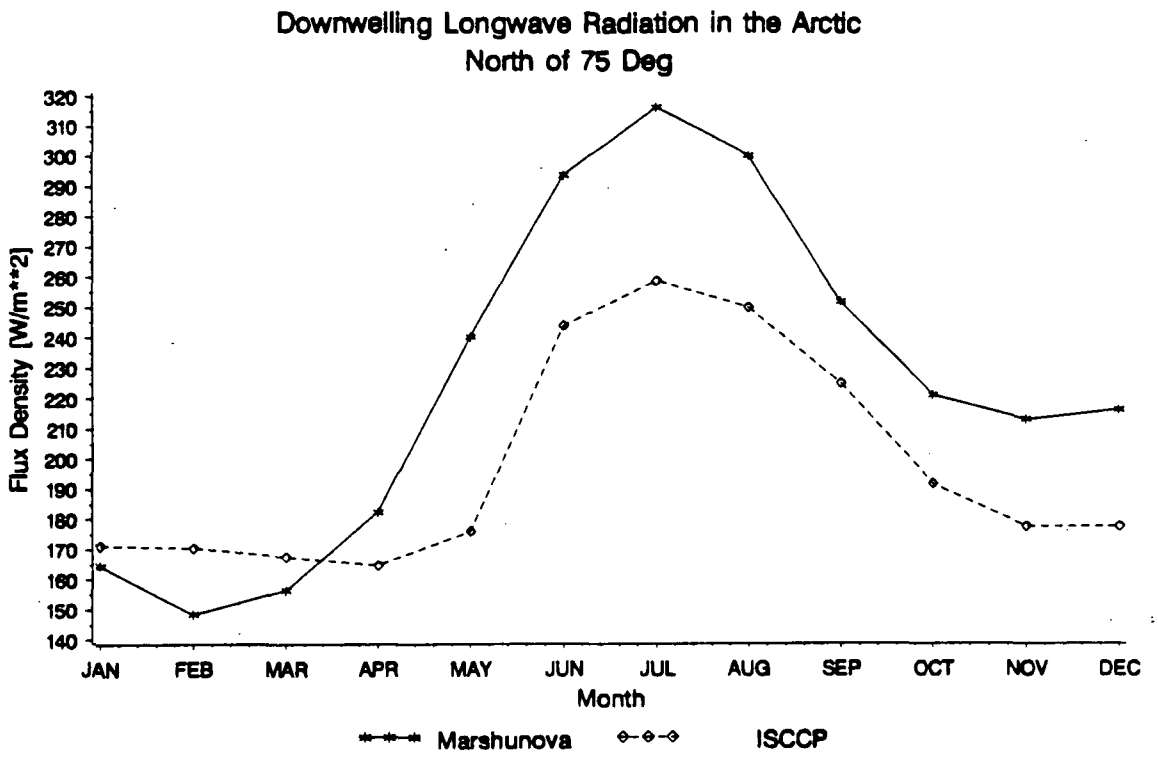

Fig. 5.7 Comparison of the spatial patterns of downwelling shortwave flux-densities at the surface $R_S\downarrow$ compared with flux-densities reported by *Vohwinkel and Orvig* [1962].

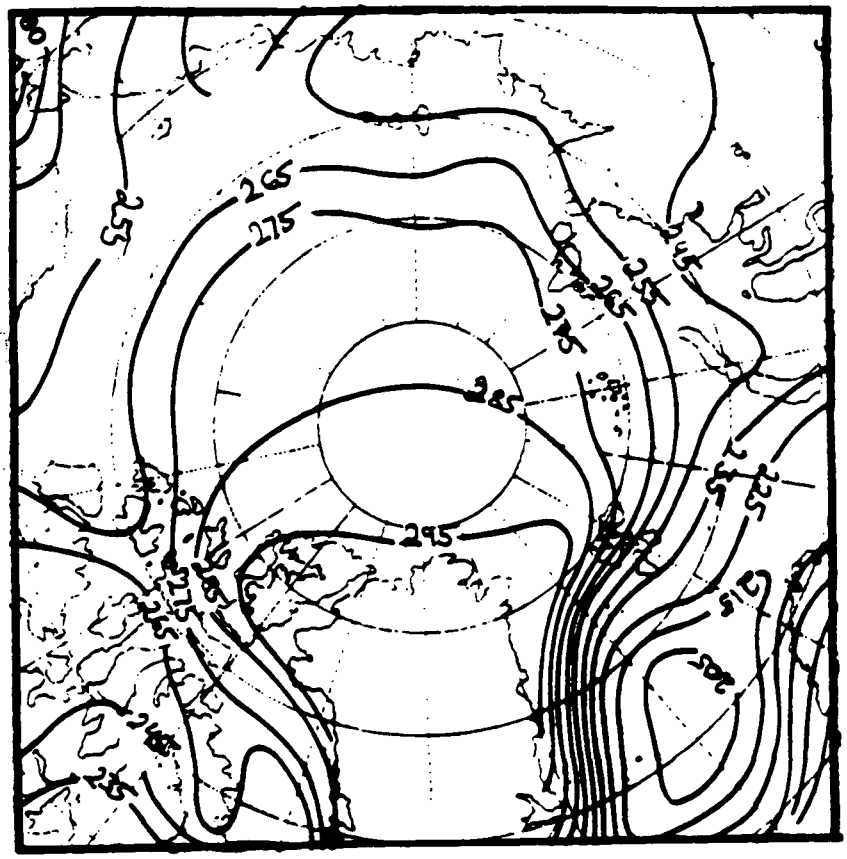

Fig. 5.8 Annual cycle of spectrally integrated surface albedo (dashed-diamond) computed from the ISCCP data set and albedoes from measurements by *Marhunova* [1961] (solid). AVHRR channel 1 (0.6 μm) are also shown for comparison.

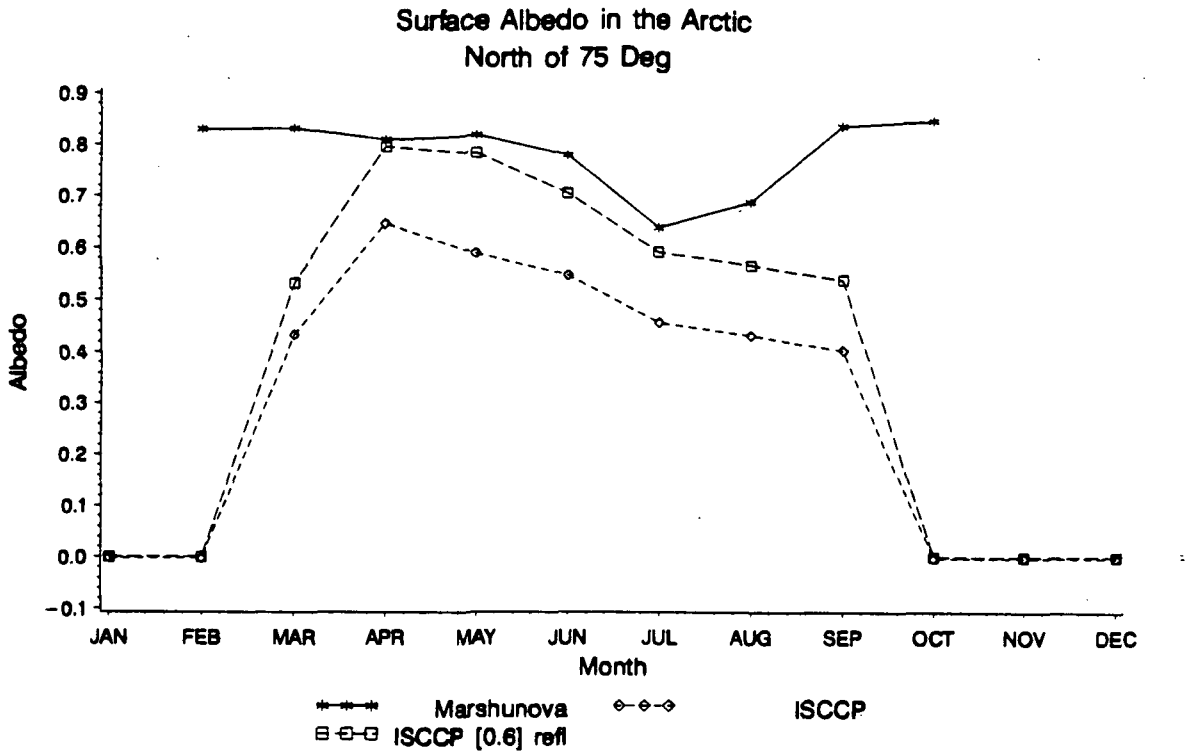

Fig. 5.9 Comparison of the spatial patterns of integrated spectral surface albedo calculated from the ISCCP data set (top) in May with those parameterized from a manual interpretation of DMSP visible imagery by *Robinson et al.*, [in press]. Note 45° rotation between figures.

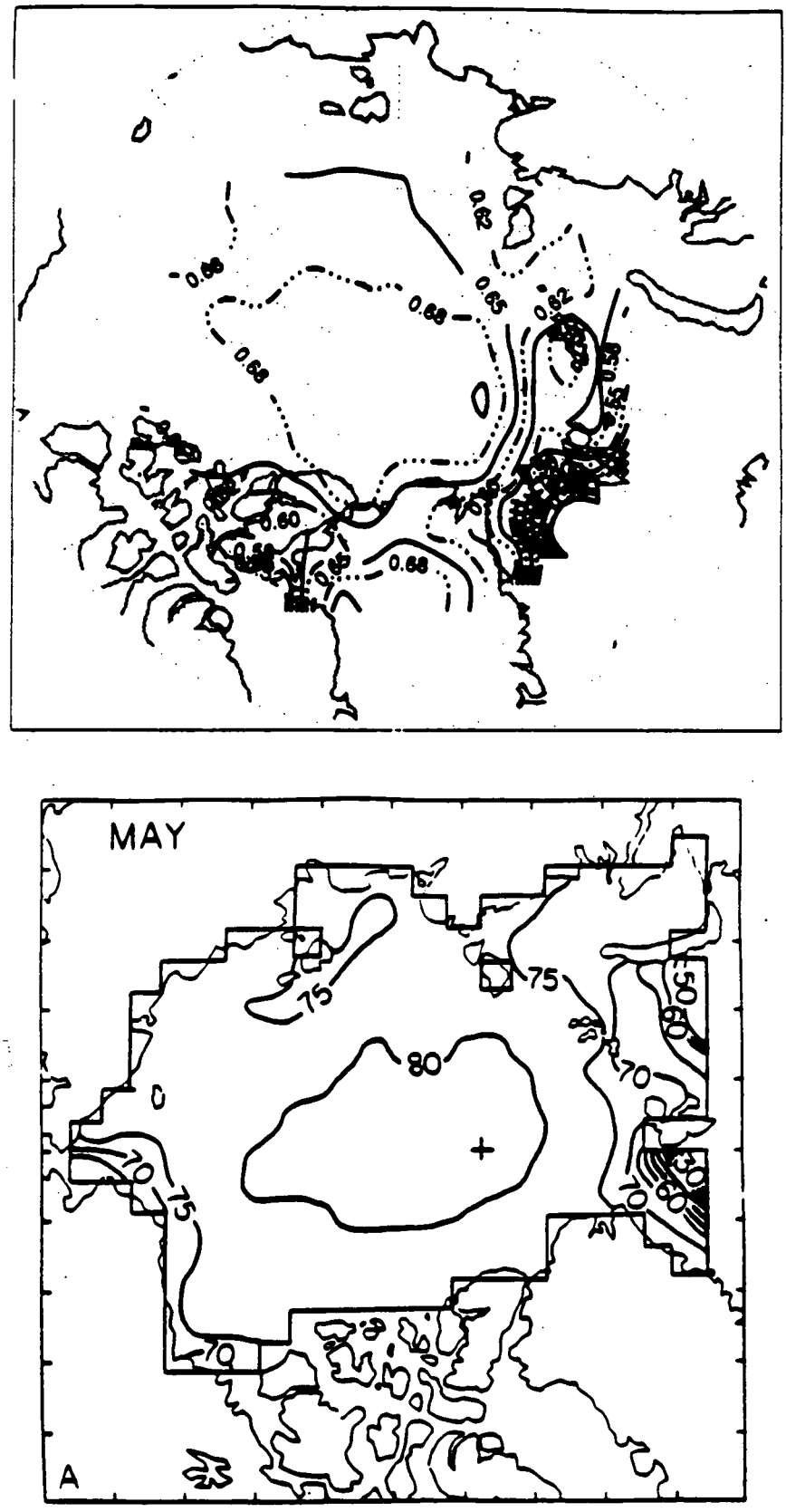

Fig. 5.10 Comparison of the spatial patterns of integrated spectral surface albedo calculated from the ISCCP data set (top) in July with those parameterized from a manual interpretation of DMSP visible imagery by *Robinson et al.*, [in press]. Note 45° rotation between figures.

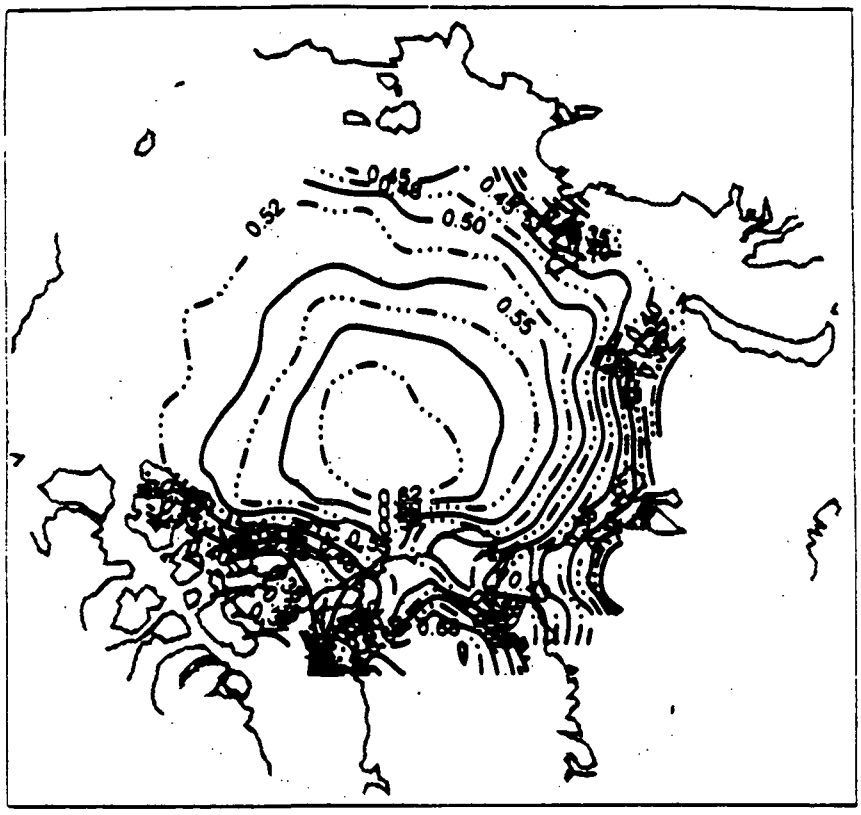

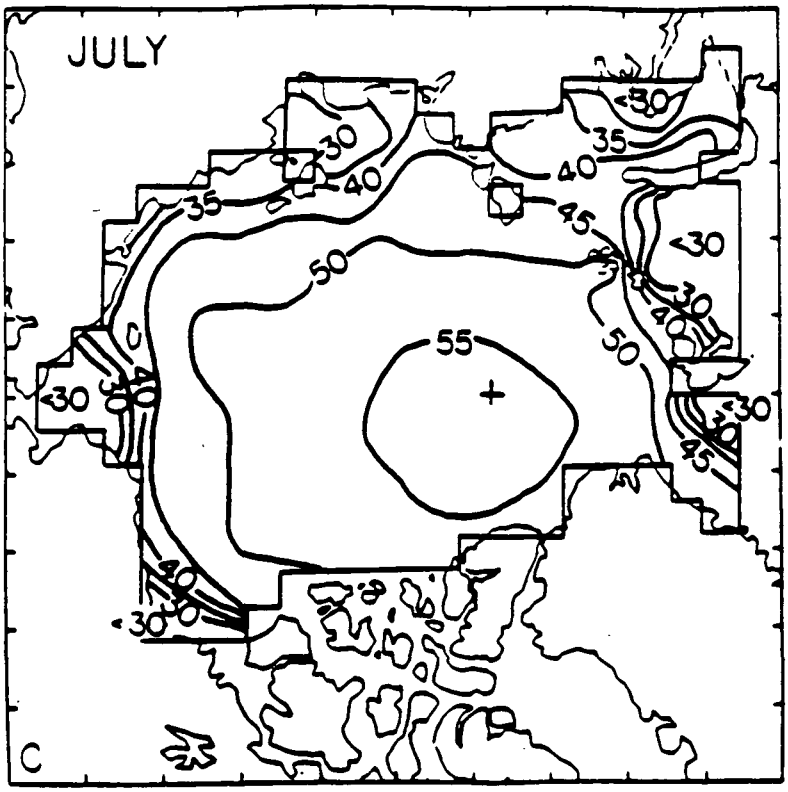

Fig. 5.11 Annual cycle of top of the atmosphere radiative fluxes calculated from the ISCCP data set. Shown are direct downwelling shortwave $R_t\downarrow$ (solid-star), upwelling shortwave $R_t\uparrow$ (dashed-diamond), upwelling longwave $L_t\uparrow$ (dashed - square), and net radiation. $N = R_t\downarrow - R_t\uparrow - L_t\uparrow$ (dashed-triangle).

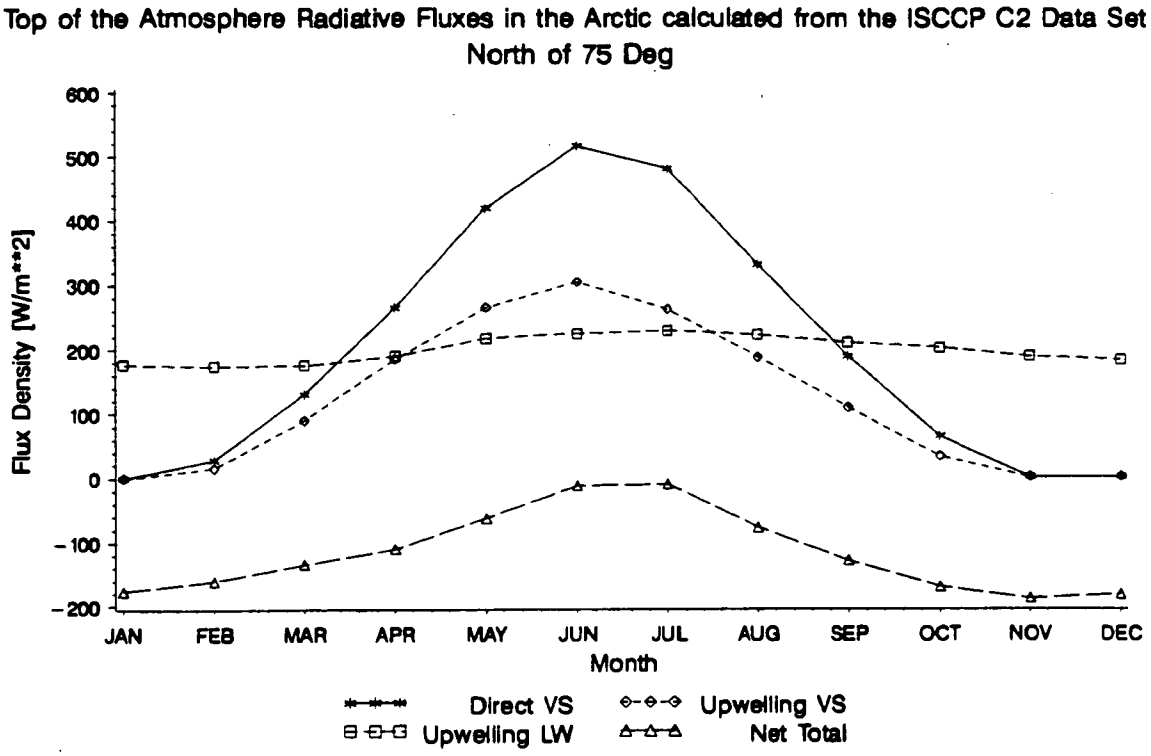

6. CLOUD DETECTION

Jeff Key

With the development of an ice surface temperature retrieval algorithm and the possibility of surface albedo retrieval from satellite data the problem of cloud detection in the AVHRR channels in particular becomes an even more urgent problem. However, the study of polar cloudiness and properties of the underlying surface using satellite data such as that provided by the AVHRR encounters a number of significant difficulties that influence the reliability of cloud retrieval schemes. Some particularly relevant ones are:

(i) Low radiance contrasts between cloudy and clear scenes: The small polar temperature lapse rates reduce the infrared radiance contrasts and the snow and ice covered surface limit the solar reflection contrasts (Fig. 2.1). Thus the radiance characteristics in polar regions require sensitive radiance analysis.

(ii) The complex surface property variations caused by changes in snow and sea ice: Rapid small-scale variations in surface properties, particularly surface reflectance, make it difficult to characterize cloud free scenes based on spatial and temporal variability techniques.

(iii) The effect of haze on reflected and emitted radiances: The presence of optically thick haze, especially during the spring in the Arctic, may obscure the pack ice and conceal discernible surface features that might otherwise be used to determine the absence of cloud layers or used in an automated retrieval scheme.

(iv) Complex non-linear relationship between radiances and cloud properties: The differences in the angular variations of reflected sunlight between rough surfaces and broken clouds and the occurrences of strong inversions produce complex effects on these relationships. The utility of simple radiance difference techniques is doubtful and cloud retrieval becomes a multi-valued problem.

The impact of these uncertainties on cloud retrieval methods will vary in degree according to location and season. However, some overall assessment of their effects on satellite radiance measurements is sorely needed. Since operational digital imagery over the polar region is only available from polar orbiting meteorological satellites of the NOAA series, assessment of these factors in the context of AVHRR might provide insight to the solution of these problems.

The cloud detection problem in polar satellite data is not trivial, however. For a review of polar cloud detection algorithms, see *Key and Barry* [1989] and *Sakellariou et al.* [in press] and the references contained therein. The current status of cloud detection from AVHRR data in the polar regions is that there are algorithms that work reasonably well (estimated accuracy to within 10%) but are not near an operational stage. The reason is that, in general, the algorithms do not have a strong basis in the physical relationships between cloud and surface characteristics and radiative transfer, but rather depend upon empirically-derived thresholds.

We therefore intend to examine analytically the transfer of radiation through polar atmospheres in order to determine exactly what can be detected in the data as well as what cannot. To

accomplish this goal we are in the process of acquiring the appropriate radiative transfer model(s). Currently there is no single model that will allow us to accurately simulate satellite sensor radiances in the polar regions. We use LOWTRAN for thermal calculations but its treatment of multiple scattering is not accurate enough for the shortwave simulations. The discrete ordinate code that is in-house does not use spherical geometry (which is important at low sun angles/large solar zenith angles). Additionally, the spectral resolution of the absorption coefficient data is too low. We are obtaining a version of this code that includes spherical geometry and are searching for higher spectral resolution absorption data. Another solution may be the use of MODTRAN, a moderate spectral resolution model like LOWTRAN. MODTRAN is currently on order. Cloud detection and analysis will be one of the major focii of Year 3.

Fig. 6.1 Bispectral plot of data from an AVHRR summer scene of the Kara Sea area. Pixel values in AVHRR channel 1 (visible) and 5 (thermal) are shown. The spectral ranges of various cloud and surface types are illustrated (rectangles) based on manual interpretation. HCL = high cloud, MCL = middle cloud, and LCL = low cloud.

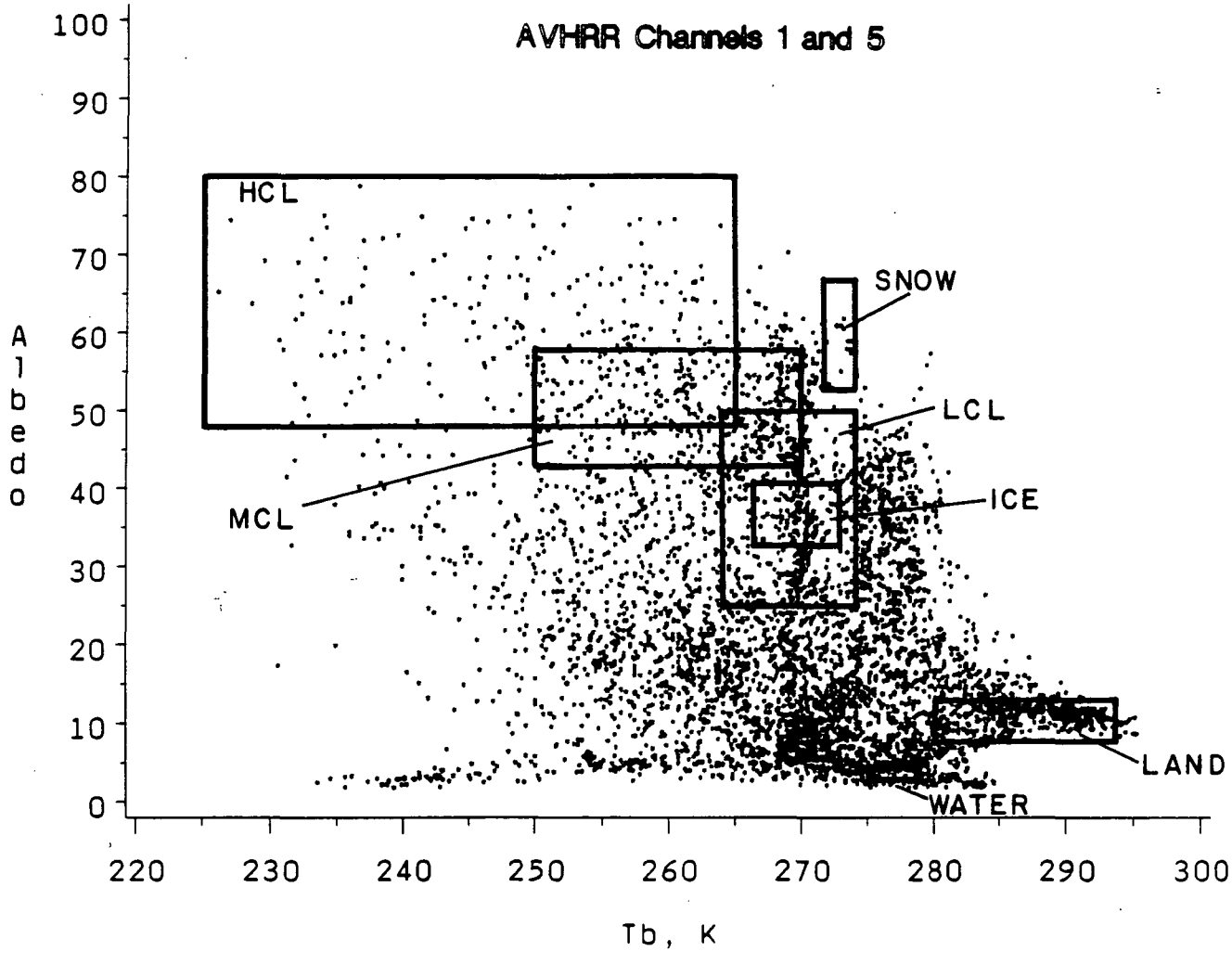

7. AVHRR AND SSM/I SOFTWARE DEVELOPMENTS

Chuck Fowler and Konrad Steffen

Work was done in three major areas; (a) installation of AVHRR navigation and processing programs, transferred from the Colorado Center for Astrodynamic Research (CCAR), University of Colorado, (b) navigation and processing of AVHRR images for Arctic regions, and (c) development of display software for passive microwave satellite data (SMMR and SSM/I) for UNIX based computers.

7.1 AVHRR Navigation Software

CCAR has developed software for processing AVHRR data. This software navigates raw satellite images to geographically gridded images, either data directly ingested from a satellite receiver or level 1b data. Previously, this software had only been tested on DEC-stations.

One task was to port the navigation routines to Sun SPARC2 computers. Because of differences in the machines, some debugging was necessary. Calibration of the AVHRR images was a major step. The calibration software had not been fully tested and several errors were found that needed to be resolved. Also, implementation of non-linear corrections were added to the calibration step. These non-linear corrections are different for each of the Tiros-N series of satellites, and are found in the NOAA user's guide. It was found that these corrections are quite important for the work we need, and results appear to be closer to expectations.

The navigation programs from CCAR are as complete as possible in terms of orbital modeling. Some mis-registration of the images and map overlays occurs and is due to poor timing data caused by drift in the satellite's on board clock. The pitch, yaw and roll of the satellite is not known and could add to an additional error for the geolocation of the individual pixels. The navigation software can process AVHRR data from different receiving stations.

7.2 AVHRR Data Processing

For one of our study areas, the Greenland ice sheet, AVHRR data from two different receiving stations (Tromso, Norway and NOARL, Mississippi).was received. The data was processed twice; once for a small area near the Davis Strait that coincides with ground station data, and also for full resolution images of Greenland itself.

The AVHRR data covered about 15 different days during 1990 and 1991. All AVHRR channels were extracted from the data for the areas of interest, registered to geographic maps, and calibrated as described in the previous section. This was done several times, after improvements were made to the calibration programs.

In addition, numerous AVHRR scenes were processed for the upcoming AVHRR IST

intercomparison workshop in Boulder, May 1992. DMSP OLS data was obtained to correspond with some of the AVHRR data over Greenland. No navigation routines were available to process this OLS data, but images were extracted from the raw data, so that the data could be displayed, even though they could not be registered with any map projection.

7.3 SSM/I Display System

Currently there is no display program for SSM/I images for UNIX-based systems such as the IMDISP program for IBM compatible computers. This IMDISP program in provided on the SSM/I CDROM's from NSIDC.

An interactive display application running under IDL developed with similar capabilities than the IMDISP program. The display software can load both SSM/I and SMMR images from the NSIDC CDROM. The images can be displayed, the color tables can be modified, and the contrast adjusted for each image..

Brightness temperatures, longitude, and latitude can be displayed at each pixel location. Ice concentration images can be created with the current hemispheric tie points provided in the NSIDC user's guide. User's will also be able to redefine their own tie points. Areas within the images can be outlined, and these regions will be used for scatter plots correlating values between the different channels. As a research tool, this will allow users to define local tie points more accurately. The maps and land masks that are provided with the CDROMs can be overlaid on the images for display purposes.

This interactive display program has not been completely finished and debugged. After the implementation of some additional options (summer 1992), the UNIX-based display software will be made available to the science community at no cost through the NSIDC-DAAC.

8. REFERENCES

Blanchet, J. and R. List, Estimation of optical properties of arctic haze using a numerical model, *Atmos.-Ocean*, 21, 444-465, 1983.

Cavalieri, D.J., P. Gloerson, and W.J. Campell, Determination of sea ice parameters with the Nimbus 7 SMMR, *J. Geophys. Res.*, 89, 5355-5369, 1984.

Chandrasekhar, S., Radiative transfer, Dover Publication, Inc., New York, 1960.

Curry J.A., and E.E. Ebert, Annual cycle of radiation fluxes over the Arctic Ocean: sensitivity to cloud optical properties. *Int. J. Climatatology* (in press).

Dozier, J. and S.G. Warren, Effect of viewing angle on the infrared brightness temperature of snow, *Water Resources Res.*, 18(5), 1424-1434, 1982.

Fletcher, J.O., The heat budget of the Arctic basin and its relation to climate. Rand Corporation Report R-444-PR. Santa Monica, 1961.

Flato, G.M. and W.D. Hibler III, On a simple sea-ice dynamics model for climate studies. *Annals Glaciol.*, 14, 72-77, 1990.

Grenfell, T.C. and G.A. Maykut, The optical propertie of ice and snow in the Arctic basin. *J. of Glaciology*, 18(80), 445-463, 1977.

Henderson, P.M., Cloud conditions over the Beaufort Sea. Publications in Meteorology No. 86. McGill University, Montreal, 1967.

Hibler, W.D. III, A dynamic thermodynamic sea ice model. *J. Phys. Oceanog.* 9: 815-846., 1979.

Huschke, R.E., Arctic cloud statistics from "air calibrated" surface weather observations. *Rand Corporation Memorandum* RM-6173-PR, 1969.

Key, J. and R.G. Barry, Cloud cover analysis with arctic AVHRR data: 1. cloud detection, *J. Geophys. Res.*, 94(D15), 18521-18535, 1989.

Kneizys, F.X., E.P. Shettle, L.W. Abreu, J.H. Chetwynd, G.P. Anderson, W.O. Gallery, J.E.A. Selby, and S.A. Clough, Users Guide to LOWTRAN 7, AFGL- TR-88-0177, Environmental Research Papers, No. 1010, 137 pp., 1988.

Mashunova, M.S., Principle Regularities of the Radiation Balance of the Underlying Surface and of the Atmosphere in the Arctic. (in Russian)., Trudy AAHUU T229, Leningrad, 1961.

Maykut, G.A., Large-scale heat exchange and ice production in the central Arctic, *J. Geophys. Res.*, 87(C10), 7971-7984, 1982.

McClatchey, R.,A.,W.S., Benedict, S.A. Clough, D.E. Burch, R.F., Calfee, K.Fox, L.S.Rothamn And J.S. Garing, AFCRL, atmospheric absorption line parameters compilation, Envrion. Res. Pap. No. 434, AFRL-TR0-73-0096, 78 pp [NTIS AD 762904], 1973.

Parkinson, C.L. and W.M. Washington, A large-scale numerical model of sea ice. *J. Geophys. Res.*, 84 (C1), 311-336, 1979.

Raschke, E., H. Cattle, P. Lemke, and W. Rossow, Report on the Workshop on Polar Radiation Fluxes and Sea-Ice Modelling. World Climate Research Programme, WMO/TD, Bremerhaven, Germany, 5-8 November, (in press).

Robinson, D.A., M.C. Serreze, R.G. Barry, G. Scharfen, and G. Kukla, Large-scale patterns and variability of snow melt and parameterized surface albedo in the Arctic basin. *J. of Climate*, (in press).

Sakellariou, N.K., H.G. Leighton, and Z. Li, Identification of clear and cloudy pixels at high latitudes from AVHRR radiances, *Int. J. Remote Sensing*, (in press).

Serreze, M.C., J.D. Kahl, and R.C. Schnell, Low-level temperature inversions of the Eurasian Arctic and comparisons with Soviet drifting station data. *J. Climate*, (in press).

Stearns, L.P., E.W. Barrett and R.F. Puechel, Effects of a power plant plume on radiative transfer. *Meteorol. Res.*, 35, 76-84, 1982.

Stowe, L.,L., C.G.Wellenmeyer,T.F. Eck, H.Y.M Yet and the Nimbus-7 Cloud Data Processeing Team, Nimbus-7 Global Cloud Climatology, Part 1 : algorithms and validations. *J. of Climate*, 1,445-470, 1988.

Swain, P.H. and S.M. Davis, (eds) Remote Sensing: The Quantitative Approach, McGraw-Hill, New-York, 1978.

Tsay, Si-Chee, K. Stamnes and K. Jayaweera, Radiative Energy Budget in the Cloudy and Hazy Arctic. *J. Atmos. Sci.*, 46(7), 1002-1018, 1989.

Vohwinkel. E., and S. Orvig, Insolations and Absorbed Solar Radiation at the Ground in the Arctic. Publications in Meterology. No.53. McGill University, Montreal, 1962.

Walsh, J.E. and H.J. Zwally, Multiyear sea ice in the Arctic: Model- and satellite-derived. *J. Geophys. Res.*, 95 (C7), 11,613-11,628, 1990.

Warren, S.G., and W.J. Wiscombe, A model for the spectral alpedo of snow II. Snow containing atmospheric aerosols. *J. Atmos.Sci.*, 37,2734-2745, 1980.

Warren, S.G., C.J. Hahn, J. London, R.M. Chervin, and R. Jenne, Global distribution of total cloud cover and cloud type amounts over land. *NCAR Technical Note* Tn-273+STR, Boulder, Colorado., 1986.

Warren, S.G., C.J. Hahn, J. London, R.M. Chervin, and R. Jenne, Global distribution of total cloud cover and cloud type amounts over the ocean. *NCAR Technical Note* TN-317+STR. Boulder, Colorado, 1988.

Wiscombe, W.J., and J.W. Evans, Exponential- sum fitting of radiative transmission functions. *J.Comput. Phys.*, 24, pp 416-444, 1977.

Wiscombe, W.J. and S.G. Warren, A model for the spectral albedo of snow. I : Pure snow. *J. Atmos. Sci.*, 37,2712-2733, 1980.

9. Papers Supported in Whole or in Part by NAGW-2158

Barry, R.G., D. Cavalieri, S. Martin, J. Maslanik, K. Steffen, R.L. Weaver, and C. Morris. Advances in sea ice research based on remotely-sensed passive microwave data, *Oceanography*, (submitted).

Emery, W.J., M. Radebaugh, C.W. Fowler, D. Cavalieri, and K. Steffen. An intercomparison of sea ice parameters computed from AVHRR and Landsat satellite imagery and from airborne passive microwave radiometry. *J. Geophys. Res.*, 96(C12), 22075-22086, 1991.

Grenfell, T.C., D. Cavalieri, D. Comiso., and K. Steffen. Microwave remote sensing of sea ice: Chapter 6 - determination of thin ice. AGU Monograph, (in press).

Key, J. and M. Haefliger. Arctic ice surface temperature retrieval from AVHRR thermal channels. Accepted for publication in *J. Geophys. Res. (Atmospheres)*, October 1991.

Key, J. and M. Haefliger. Retrieval of ice surface temperature, outgoing longwave radiation, and cloud cover from AVHRR data. WMO Report on Polar Radiation Fluxes and Sea Ice Modeling, WMO/TD, C22-C28, (in press).

Maslanik, J.A., and J. Key, Fetch and stability sensitivity in large-area estimates of turbulent heat flux over sea ice, *submitted to J. Geophys. Res.*

Schweiger, A.J. and J. Key. Comparison of ISCCP-C2 and Nimbus-7 satellite-derived cloud products with a surface-based cloud climatology in the arctic. Accepted for publication *J. Climate*, February 1992.

Seelye, M., K. Steffen, and. D. Cavalieri. Microwave remote sensing of sea ice: Chapter 16 - Microwave remote sensing of polynyas. AGU Monograph (in press).

Steffen, K., Energy flux density estimation over sea ice based on satellite passive microwave measurements, *Annals of Glaciology*, 15, 178-183, 1991.

Steffen, K. and A. Schweiger. NASA team algorithm for sea ice concentration retrieval from Defense Meteorological Satellite Program special sensor microwave imager: comparison with Landsat satellite data. *J. Geophys. Res.*, 96(C12), 21971-21987, 1991.

Steffen, K., et al., Microwave remote sensing of sea ice: Chapter 9 - passive microwave algorithm. AGU Monograph, (in press).

Steffen, K., and A. Schweiger. Application of passive microwave satellite data in arctic climate research. Glaciological Data, World Data Center A for Galciology, Univ. of Colorado at Boulder, (in press).

10. Conference Presentations Supported in Whole or in Part by NAGW-2158

Haefliger, M. and J. Key. Sea ice surface temperature retrieval from AVHRR thermal channels. American Geophysical Union, San Francisco, December 9-13, *EOS*, October 29, 170, 1991.

Schweiger, A., J. Key, and M. Haefliger. Arctic radiative fluxes and cloud forcing estimated from the ISCCP C2 cloud data set, 1983-1986. American Geophysical Union, San Francisco, December 9-13, *EOS*, October 29, 238, 1991.

Steffen, K. SSM/I NASA algorithm sea-ice retrieval comparison with Landsat satellite and aerial photography for the Bering Sea. *2nd WMO Workshop on operational remote sesning of sea ice.* Microwave Group, Center for Research in Experimental Space Science, York University, Canada, 52, 1991.

Steffen, K. Monitoring radiative fluxes and surface properties of the Greenland ice sheet. American Geophysical Union, San Francisco, December 9-13, *EOS*, October 29, 150, 1991.